GSK-3 regulates CD4-CD8 cooperation needed to generate super-armed CD8+ cytolytic T cells against tumors

Bastien Moës[1-3], Janna Krueger[1-3], Alexandra Kazanova[1-3], Chen Liu[1-3], Yunfeng Gao[1-3], Nikhil Anto Ponnoor[1-3], Linda Castoun-Puckett[1-3], Andres Carlos Oroya Lazo[1-3], Lan Huong[1-3], Auryane Laure Cabald[1-3], Thai Hien Tu[1-3] and Christopher E. Rudd[1-6]

[1]Department of Medicine and Sciences biomédicales, Université de Montréal, Montréal, QC H3C 3J7, Canada; [2] Dept de microbiologie, infectiologie et immunologie, Université de Montréal; [3]Cell Signaling and Immunotherapy Section, Research Center Hopital Maisonneuve-Rosemont (CR-HMR) Montreal, Quebec H1T 2M4; [4]Department of Medicine, McGill University;[5]Institut universitaire d'hématologie-oncologie et thérapie cellulaire (IHOT); [6]Department of Medicine, McGill University, Montreal, Canada

Short title: GSK-3 regulates CD4-CD8 cooperation and synergy with anti-PD-1 immunotherapy

Corresponding author: Christopher E Rudd

Abstract

While immune checkpoint inhibitor therapy has transformed cancer treatment, the signaling pathways underlying T-cell function optimization remain incompletely understood. While glycogen synthase kinase-3 (GSK-3) is a negative regulator and CD4+ T-cells provide help for CD8+ T-cell development, the signaling events controlling CD4-CD8 T-cell cooperation are unclear. Here, using GSK-3 knock-down mice (GSK-3KD), we show that GSK-3 is the central regulator of CD4-CD8 cooperation, specifically in enhancing the expression of granzymes necessary for CD8+ CTL killing. GSK-3KD induced metabolic reprogramming toward glycolysis in T-cells and, when combined with PD-1 blockade, overcame tumor checkpoint resistance characterized by reduced Treg TILs and increased effector-memory CD8+ TILs. GSK-3KD with anti-PD-1 therapy induced unprecedented expression of seven out of nine granzymes in CD8+ TILs through enhanced CD4+ T-cell help. These findings identify GSK-3 as a key regulator of CD4+ T-cell help in generating highly cytotoxic CD8+ T-cells, presenting a promising therapeutic strategy for cancer treatment.

Introduction

Antigen presenting cells, helper and suppressor T-cells as well as memory and effector subsets orchestrate the nature and amplitude of the response[1]. In this context, CD4+ and CD8+ T-cells are the key players of the adaptive immune response, working together to eliminate infected or cancer cells [2, 3]. CD4+ T-cells deliver essential signals for CD8+ T-cells, allowing them to develop into long-lasting memory cells and cytotoxic effector cells capable of eliminating infected or cancerous cells [5,7]. Without this support, CD8+ T-cells may become dysfunctional, impairing their ability to control viral infections[4, 5, 6]. CD4+ T-cells facilitate CD8+ T-cell activation through various mechanisms, including the production of cytokines such as IL-2, IFN-γ, and TNF-α, and by enhancing dendritic cell function through upregulation of co-stimulatory molecules. Conversely, regulatory T-cells (Tregs) play a crucial role in maintaining immune tolerance and suppressing anti-tumor immune responses[7]. Moreover, manipulating CD4+ T-cell help and Treg activity is a promising strategy for cancer immunotherapy[8, 9]. Further, the continuous exposure to antigens can cause exhaustion, impairing the clearance of pathogens and tumors[10,11, 12]. In this context, inhibitory co-receptors such as cytotoxic T-lymphocyte antigen 4 (CTLA-4), programmed death-1 (PD-1), and lymphocyte-activation gene 3 (LAG-3) limit T-cell responses[13]. The blockade of these receptors by antibodies has proven to be a promising approach for the treatment of several cancers[14,15, 16, 17, 18, 19]. The transcription factor, T cell factor 1 (TCF-1) also defines memory T cell precursors while its absence is associated greater effector function[20, 21, 22, 23]. TCF-1+ T-cells are essential for successful anti-tumor response in checkpoint blockade immunotherapy [24, 25, 26]. Effector cytolytic T-cells (CTLs) release cytotoxic granules that contain perforin and granzymes (GZMs) needed to induce apoptosis in target cells[27, 28]. Although, granzyme B (GZMB) is the best studied GZM, 9 other GZMs are expressed in mice that act on overlapping and unique protein substrates in the targeting of cells[29, 30, 31, 32].

T-cell activation is mediated by an array of protein-tyrosine, serine/threonine and lipid kinases as well as GTP binding proteins and downstream substrates induced by the engagement of the antigen-receptor and co-receptors[33, 34, 35,36, 37]. As we first showed, activation is initiated via the CD4 or CD8 co-receptors and their ability to bind to the protein-tyrosine kinase[38,36]. $p56^{lck}$ phosphorylates the T-cell receptor (TCR) associated CD3 and ζ chain immunoreceptor tyrosine-based activation motifs (ITAMs)[38,36]. This leads to the recruitment of a second zeta-chain-associated protein kinase 70 (ZAP-70)[39]. $p56^{lck}$, either

receptor bound or free, phosphorylates a wide array of downstream substrates[36], while ZAP-70 phosphorylation is more restricted in phosphorylating adaptors such as SH2 domain containing leukocyte protein of 76kDa (SLP-76)[40] and linker for activation of T cells (LAT)[37].

Glycogen synthase kinase-3 (GSK-3) is a serine/threonine kinase that is unusual in this its is constitutively active in quiescent T-cells and becomes inhibited in response to receptor ligation [41, 42]. It phospho-inhibits glycogen synthase[43], generating signals, in part, via β-catenin generation [44, 45, 46]. In mammals, two isoforms of GSK-3 have been identified: a 51 kDa GSK-3α isoform and a 47 kDa GSK-3β isoform encoded by separate genes[47]. Unlike most kinases, the inactivation occurs through the phosphorylation of specific serine residues (Ser9: GSK-3β, Ser21: GSK-3α). This phosphorylation enables the phospho-serine tail of GSK-3 to bind and obstruct its own active site [48, 49]. By contrast, tyrosine phosphorylation of GSK-3 (Tyr216: GSK-3β, Tyr279: GSK-3α) enhances kinase activity [50, 51]**.** Both isoforms are expressed in numerous tissues [52] and regulate diverse processes from glycogen metabolism to microtubule stability [50, 53]. The β isoform has been implicated in diabetes [54], Alzheimer disease [55], and inflammation [56]. In the context of tumor immunity, we have shown that GSK-3 inactivation can downregulate PD-1 and LAG-3 transcription[57, 58] and can be effective in controlling tumor growth[59, 60, 61, 57, 58, 59, 62, 63]. FDA approved studies using GSK-3 inhibitors such as Elraglusib (9-ING-41) are now being used to treat various cancers [64, 65].

Despite its potential importance, the full role of GSK-3 to immune function has yet to be explored. Here, we show for the first time that GSK-3 controls CD4-CD8 T-cell crosstalk in synergy with anti-PD-1 to generate super-armed CD8+ effectors in immunotherapy. The genetic downregulation of GSK-3 promoted progenitor and memory CD8+ T-cells as well as markedly decreasing the presence of suppressor Tregs. Further, GSK-3 downregulation, combined with anti-PD-1, unlocked an extraordinary cytotoxic potential in CD8+ T-cells, enabling the expression of an unprecedented 7 out of 9 granzymes from the mouse genome, a phenomenon not before observed. This newly uncovered GSK-3-dependent CD4-CD8 T-cell crosstalk mechanism provides a transformative approach to enhance anti-PD-1 immunotherapy.

Results

GSK-3 KD mice show increased memory-TCF-1 expression in response to Cl 13 LCMV

To define the role of GSK-3 in T-cell biology in different infection context, we first crossed distal promotor *lck*-Cre mice (i.e. *dlck*-Cre) with *gsk-3α* $^{lox/flox}$ *β* $^{flox/flox}$ mice to deplete GSK-3 in mature T cells. The distal promoter allows deletion primarily in peripheral T-cells avoiding effects on thymic selection[66]. Immunoblotting showed that a greater than a >70% reduction GSK-3α and GSK-3β in splenic T cells (Fig. 1A) (referred to as GSK-3 knock-down (KD) or dLCK-CRE). We next assessed how GSK-3 KD influences the responses to infection using chronic Cl 13 and acute Armstrong stains of LCMV, as described[57, 67]. In the case of Cl 13, the dLck-CRE GSK-3 KD mice showed less weight loss from days 0-8 and a more rapid and complete recovery from day 10-30 than wild type mice (Fig. 1B). No difference in the weight was observed following acute infection with LCMV Armstrong (Fig. 1C). Further, the number of CD8+ T-cells in the spleens of the GSK-3KD mice was significantly higher than in wild-type mice 30 days after infection with the Cl13 strain of LCMV (Fig. 1D). A similar trend was seen after infection with the Armstrong strain of LCMV at day 7. Additionally, GSK-3KD mice had greater numbers of effector memory (GP33+CD44+CD62L-) and central memory (GP33+CD44+CD62L+) CD8+ T-cells in response to Cl13 infection (Fig. 1E). Tetramers with the GP33 peptide of amino acids 33-41 from the LCMV glycoprotein allows a more specific recognition of responses specific to the viral infection. By contrast, the numbers of GP33+ KLRG1+CD39+ terminal effector cells (TE) were reduced in GSK-3KD mice (Fig. 1F). Following infection with the Armstrong strain of LCMV, dLCK-CRE mice also exhibited a higher number of effector memory cells compared to wild-type mice at 7 days post-infection, while central memory cells were not detectable at this 7-day time point (Fig. 1G). These data demonstrate that reduced GSK-3 expression promotes the differentiation of CD8+ T-cells, as evidenced by an increase in the numbers of effector memory and central memory T-cells in response to infection.

In terms of other cellular subsets, we also observed elevated numbers of total CD4+ T-cells, CD44+CD4+ T-cells, and CD44+Gp33+CD4+ T-cells in GSK-3KD mice relative to controls as well as Th1, Th2 and FoxP3 Tregs (Fig. S1). In addition, we observed an increase in total B cells, CD44+ B cells, and CD44+GP33+ B cells in GSK-3KD mice compared to controls as well as germinal center CD44+ B-cell numbers in GSK-3KD mice (Fig. S2). Cell populations were identified using anti-CD19, CD44, and GP33 tetramer staining.

In terms of CD8+ T-cells, GSK-3 KD mice also showed an increase in the percentage of GP33+TCF-1+ CD8+ T-cells within the CD44+ pool of experienced T-cells (Fig. 1H). We also observed an increase of TCF-1+ cells in the central and effector memory CD8+ compartments. of TCF-1+ expressing GP33+CD44+ TEM cells from 7-15 percent was observed. Following the same theme, GSK-3 KD mice gave rise to greater numbers of memory precursor effector cells (MPECs) relative to short-lived effector cells (SLECs) when compared to WT mice (Fig. 1I). MPECs were defined as KLRG1- IL7Rα+ while SLECs were defined as KLRG1+IL7Rα-. A FACs plot of a representative experiment showed an increase in MPECs (i.e., 27.1 to 39.2) in GSK-3 KD compared to WT mice. Conversely, there was a corresponding decrease in SLECs (Fig. 1J). The MPEC population also showed a higher level of TCF-1+ expression in the GP33+ subset as measured by numbers of cells (Fig. 1K) or by precent presentation (Fig. 1L) as seen in a FACs plot of a representative experiment, an increase from 33.6% in WT to 55.8% in GSK-3KD MPECs was observed (left panels). Only marginal changes were seen in the SLEC cells. Further, MPECs from GSK-3 KD mice showed a greater increase in expression of the cell cycle marker Ki67 than seen in WT mice (Fig. 1M, upper panel). Ki67 is marker for cell division[68] .The shorter lived SLECs also showed the presence of dividing cells but they were similar in WT and KD mice (lower panel).

Then increase in progenitor-like T-cells was also reflected in a reduction in T-cell exhaustion. These stages include progenitor PD-1+TCF-1+TIM3- cells which develop into transitionary cells (PD1+TIM3+CX3CR1+) and finally into terminally exhausted (PD1+TIM-3+CX3CR1-CD101+) cells[69, 70]. The expression of TIM3 was significantly reduced in GSK-3 KD GP33+ CD8+ T-cells, although no effect on PD-1 was seen (Fig. 1N). Nevertheless, exhausted T-cells are characterized by high levels of TIM3 with reduced effector functions such as decreased cytokine production and cytotoxicity [69, 71]. In terms of GP33+ PD-1+ T-cells, we observed an increase in stem-like TCF1+ progenitors concurrent with a reduction in the both transitory and terminal exhausted CD8+ T-cells (Fig. 1O). The same TCF-1+ progenitors also showed an increase in cell division as shown by Ki67 expression (Fig. 1P). These data show for the first time using a genetic knock-down model that GSK-3 plays a central role in the generation of stem-like progenitors and T-cell exhaustion in response to 30 day+ chronic viral infection.

GSK-3KD induces metabolic reprogramming toward glycolysis in T-cells

Increase generation of CD8+ memory in dLCK-CRE infected mice suggested that GSK-3 might control the sensitivity of T-cells to a lower strength TCR signal. To assess this, CD8+ T-cells were labelled with Tag-it and incubated in vitro with a titration of soluble anti-CD3 antibodies from a range of 0.005 to 2ug/ml over 48-62 hours (Fig. 2A). Under these conditions, remarkably, CD8+ T-cells from GSK-3KD mice showed an ability to proliferate to 0.005ug/ml (see arrow). No proliferation was observed in wild-type CD8+ T-cells at this concentration. A similar result was obtained when we stained for Ki67, a marker for cell division (Fig. 2B). Again, an increase in expression was seen at 0,005 ug/ml anti-CD3e in CD8+ T-cells from dLCK-CRE mice but not WT mice. This clearly demonstrated that GSK-3 controls the sensitivity of T-cells to anti-CD3 induced activation.

The activation of T-cells is accompanied by a switch from oxidative phosphorylation to glycolysis[72, 73, 74, 75]. The role of GSK-3 in the process has not been examined. To this end, a measurement of oxygen consumption rate (OCR) and extracellular acidification rate (ECAR) were assessed in resting and anti-CD3 stimulated T-cells at 24 hours using Seahorse XF24 Extracellular Flux Analyzer (Fig. 2C-K). Cells were subjected to the sequential addition of mitochondria perturbing agents such as oligomycin, to block ATP synthesis, FCCP to uncouple the electron transport chain, and rotenone and antimycin A which block ETC complex I and III, respectively). ECAR as a measure of glycolysis as shown in a representative experiment (Fig. 2C). Both basal and anti-CD3 induced glycolysis with the addition of exogenous glucose was higher GSK-3 KD T-cells than WT cells. However, the distinction was further evident with oligomycin where GSK-3 KD cells showed a major increase in glyolysis relative to the wild-type control. Comparative measurements from different mice confirmed the significant difference in glycolysis in response to anti-CD3 (Fig. 2D). Similarly, the glycolytic capacity in the GSK-3KD T cells was also higher in response to anti-CD3 (Fig. 2E). In addition, the glycolitic reserve, as indicated by the difference between the maximal ECAR after glucose and oligomycin addition and maximal ECAR after glucose injection only, was also augmented in response to anti-CD3 (Fig. 2F). These data showed that the reduction of GSK-3 expression augmented glycolysis as induced by anti-CD3e.

Mitochondrial respiration (i.e., OXPHOS) as assessed by the OCR response was also measured (Fig. 2G-K). Basal OCR levels was higher in GSK-3 KD T-cells (Fig. 2G, H). The addition of oligomycin inhibited OXPHOS while the injection of carbonyl cyanide-4 (trifluoromethoxy) phenylhydrazone (FCCP) as a disruptor of ATP synthesis through uncoupling the proton gradient generated by the mitochondrial membrane produced

maximal OCR response. Basal and anti-CD3 induced OCR was higher the GSK-3 KD cells (Fig. 2G), while no difference in the maximal respiration OCR between GSK-3 KD and WT cells was seen (Fig. 2H). Spare respiration capacity,as indicated by the difference between the maximal OCR (after FCCP injection) and basal OCR was actually decreased in anti-CD3e cells from GSK-3 KD mice (Fig. 2J). In keeping with this, an increase of ATP production but a reduction in the OCR/ECAR ratio was observed in T-cells from GSK-3 KD mice (Fig. 2K, L).

In keeping with this, Glucose Transporter-1 (GLUT-1) expression was seen to be higher on GSK-3 KD cells (Fig. 2M, N). Glucose uptake is control mainly in T-cells by GLUT-1 which is increased upon TCR activation[76, 77, 78]. Interestingly, the difference in glucose uptake and GLUT-1 expression in GSK3 KD vs WT cells was preferentially affected CD8+ T-cells (Fig. 2O and P, respectively). This reinforces the notion that GSK-3 preferentially effects CD8+ T-cells. Lastly, the increase in GLUT-1 expression (as well as CD44 and GZMB) was seen in GP33+ CD8+ MPECs (Fig. 2Q). No difference was seen in GP33+ CD8+ SLECs (Fig. 2R). Together, these findings suggest that GSK-3 KD causes T-cells to operate closer to their maximum respiratory capacity under normal conditions. The lower OCR/ECAR ratio indicates these cells may be more reliant on glycolysis relative to oxidative phosphorylation for their energy needs. Glucose uptake and Glut 1 expression confirm greater increase in GSK-3 KD cells, where CD8+ T-cells and in addition GP33+ CD8+ MPEC were preferentially affected.

GSK-3 empowers anti-PD1 to overcome tumor resistance

Given these effects, we next turned our attention to the role of GSK-3 in regulating CD4+CD8+ T-cell cooperation, where CD4+ T cells provide help needed for CD8+ T cell activation and differentiation[57]. A potential role for GSK-3 in this cooperation or in overcoming tumor resistance to immunotherapy has not been explored. For this, we derived and used a specific B16-F10 melanoma subclone (B16-F10 R1), which we isolated from nutrient-deprived conditions, and which demonstrates resistance to anti-PD-1 treatment. B16-F10 R1 cells were injected intradermally followed by intra-peritoneal injections of SB415286 (GSK- 3 SMI), anti-PD1 or SB415286/anti-PD1 every 4 days (Fig. 3A). While neither anti-PD-1 nor SB415286 monotherapy affected tumor growth, the combination anti-PD-1 and SB415286 synergized to reduce tumor growth from days 8-14 based on tumor volume (Fig. 3B) and

tumor weight (Fig 3C). Spider-graphs show reduced volume growth of individual tumors in mice (Fig. 3D, upper panels). In addition, 65% of mice bearing B16-F10R1 tumors became responsive to combination therapy as opposed to non with monotherapy (Fig. 3D, lower panels).

With this, we next investigated the composition of TILs using Time-of-Flight (CyTOF) mass cytometry which employed a panel of 15 monoclonal antibodies (Fig. 3E-L). From this, we defined 20 distinct cellular subsets within the anti-TCRβ population as shown with phenograph (Fig. 3E), heat map (Fig. 3F) and boxplots representations (Fig. 3G). However, although there were various upward and downward trends, only two clusters achieved statistical significance (<0.05) (Fig. S3). This included a decrease in the presence of CD4 cluster 1 with the CD4+FoxP3+CD25+CD73+ suppressor phenotype (CD4+CD44+ CD25+, FoxP3+, CD73+, PD-1+LAG3+ IA-IE+CD49F+PDL1+) (0.04). Concurrently, the second significant grouping was an increase in cluster 20 which corresponded to a CD8+ subset (CD8+CD44+IA-IE+CD11b- and PDL1+) (0.013). This CD8+ subset was negative for PD-1 and LAG-3 suggesting an absence of transitory or terminal exhaustion (Fig. 3F).

We then employed standard flow cytometry to complement CyTOF showing an increased presence of CD8+ TILs with anti-PD-1 alone (Fig. 3H), as reported[79]. From this combination, we observed an increase in effector-memory (EM) $CD8^+$ T-cells ($CD44^+$ $CD62L^-$) with combination therapy (Fig. 3I). Importantly, increased frequency of CD8+ EM T-cells correlated with a reduced tumor size (Fig. 3J). Amongst the CD4+ population, both CyTOF and standard flow confirmed a decrease in the Treg CD4+$FOXP3^{hi}$ CD25+ CD73+ subset, a highly suppressive Treg population[80, 81]. (Fig. 3L). A significant phenotypic shift was also observed in responsive tumors following combination therapy, characterized by a notably increased ratio of CD8+ T-cells to CD4+ Tregs from within the tumor microenvironment (SFig 4).

GSK3 regulates CD4-CD8 cooperation needed for enhanced CD8+ CTL TILs

Given this finding with a special reference to CD8+ effector-memory T-cells, we next assessed gene expression based on transcriptome profiling (Figs. 4A-C). With a cutoff of an at least 2-fold increase in expression with a p-value of p<0.01, a Venn diagram depiction of genes showed multiple genes altered in conditions of GSK-3 SMI inhibition monotherapy, anti-PD-1 monotherapy and combination therapy in non/poorly responsive and high responsive tumors (Fig. 4A). Responsive tumors were defined as those with a >than 50%

reduction relative to the mean for untreated mice. Volcano plots showed an increase and decrease in expression of different genes (x-axis shows the change magnitude while the y-axis shows statistical significance). Anti-PD-1 checkpoint blockade induced a reduction in the expression of genes and combined therapy showed an array of positively and negatively regulated genes. This demonstrated that GSK-3 inhibition licenses anti-PD-1 to more fully alter the range of altered gene transcription in immunotherapy.

Employing a more stringent criterion of at least 2-fold altered expression with a significance threshold of $p < 0.001$, Volcano plot analysis revealed limited gene induction by GSK-3 SMI inhibition alone (Fig. 4B). In contrast, anti-PD-1 monotherapy significantly impacted the expression of numerous genes, primarily resulting in downregulation. Notably, only two genes, FasL and Gm8369, exhibited positive induction upon anti-PD-1 treatment (Fig. 4B, upper panel). By contrast, anti-PD-1/GSK-3 SMI combination therapy synergistically induced many more genes in a positive and a negative fashion (lower panel). Amongst the upregulated 37 genes, a remarkable induction of perforin and 7/9 granzymes in the mouse genome was induced (Fig. 4C). These included granzymes, GZMK, GZMG, GZME, GZMF, GZMD, GZMB and GZMC needed for optimal CD8+ CTL killing function (Fig. 4D). To our knowledge this effect is unprecedented. Perforin is a pore forming cytolytic protein found in the granules of CTLs, while granzymes enter via perforin to induce cell death [82, 83].

Although each of these components likely contributes to the overall cytolytic capacity of CTLs, we further investigated their expression in non-poor responders compared to high responders (Fig. 4E, F). While TILs in the poorly responding mice expressed GZMG, GZME, GZMF, and GZMD, we observed no significant increase in GZMK, GZMB, or perforin expression. Perforin, a critical pore-forming protein essential for CTL-mediated cytotoxicity, resides within cytotoxic granules and is influenced by PD-1 internalization[19]. Furthermore, GZMB has been previously demonstrated to play a pivotal role in CD8+ T cell effector function of TILs[84].

To test whether the other less known granzymes could affect CD8+ T-cell mediated killing, we used siRNA to down-regulate GZM D and F (Fig. 4G). OT1 T-cells were activated with anti-CD3/CD28 for 24 hours, then electroporated with siRNAs targeting both GZMD and GZMF, two of the lesser known GMZs[85]. Cytotoxic CD8+ T cells were cultured for 48 hours before undergoing a killing assay against EL4 target cells, as previously described. A control siRNA with a fluorescent label (FITC-scrambled) had minimal impact on killing activity. In contrast, siRNAs targeting GZMD and GZMF significantly reduced killing by more than 20%

compared to the FITC-scrambled control and cells without RNA transfection (mock). These findings confirm the essential roles of GZMD and GZMF in the killing efficiency of cytotoxic CD8+ T cells. Furthermore, building upon the previous analysis of TCF-1+ stem-like T cells, the combined treatment of anti-PD-1 and GSK-3 SMI significantly increased *tcf7* expression (Fig. 4H).

These findings were further corroborated by comparing WT and GSK-3 KD mice (Fig. 5). While anti-PD1 immunotherapy failed to significantly inhibit B16 F10 R1 tumor growth in WT mice, it resulted in a greater than 75% growth inhibition in dLCK-CRE mice at day 16 post-implantation. This was evident in both tumor volume (Fig. 5A) and tumor weight (Fig. 5B). Analysis of tumor-infiltrating lymphocytes (TILs) revealed a significant increase in the proportion of CD8+ TILs in dLCK-CRE mice compared to WT mice. Flow cytometry analysis of a representative experiment (Fig. 5C) showed that anti-PD1 increased the frequency of CD8+ TILs from 37% to 46% in WT mice, while this increase was further augmented to 60% in GSK-3 KD mice. Furthermore, the total number of CD8+ TILs per gram of tumor nearly doubled in GSK-3 KD mice. In contrast, the number of CD4+ TILs remained largely unchanged or slightly decreased (Fig. 5D).

FACs staining of granzymes showed that the use of anti-PD-1 in GSK-3 KD mice significantly upregulated the expression of perforin and multiple granzymes, GZMA, GZMB, GZMC, and GZMF, as assessed by available anti-granzyme antibodies (Fig. 5E). Other GZMS did not have suitable antibodies which worked in flow cytometry. While anti-PD1 monotherapy resulted in an increased frequency of GZMB-expressing CD8+ T-cells in WT mice, combination of anti-PD-1 on a GSK-3 KD mice significantly upregulated the expression of perforin, GZMA, GZMB, GZMC, and GZMF in terms of mean fluorescence intensity (MFI) of expression (upper panel) and the percentage of CD8+ T-cells expressing each granzyme (lower panel). These data demonstrate that GSK-3 inhibition synergizes with anti-PD1 therapy to enhance the cytotoxic capacity of CD8+ T-cells by upregulating the expression of a broad spectrum of granzymes, thereby facilitating more effective tumor eradication.

GSK-3 controls CD4+ help in the generation of CD8+ T-cells with multiple GZMs

Given this, a key next question was whether the synergistic eradication of tumors and the induction of multiple GZMs due to the reduced presence of GSK-3 reflected a regulatory effect of GSK-3 on the cooperation between CD4+ and CD8+ T-cells (Fig. 6). The relative presence

of CD4+ TILs showed a decreased trend in response to anti-PD-1 in WT and GSK-3 KD mice (Fig. 6A). In terms of the expression of Tregs, as shown in the FACs profile in the representative experiment, anti-PD-1 therapy induced an increase in the presence of CD4+ FoxP3+ regulatory TILs in WT mice (i.e., 59.8% of CD4+ CD44+ TILs), as reported by others[86, 87, 88, 89]. By contrast, as seen previously with CyTOF analysis involving combination therapy (Fig. 3F), anti-PD-1 mediated a decrease in Tregs in GSK-3 KD mice (i.e., to 26.2%) (Fig. 6B). In relative terms, GSK-3 KD mice showed an increase in FoxP3- helper T-cells in response to anti-PD-1. These findings strengthen our previous CyTOF analysis by demonstrating in a genetic knockdown model that GSK-3 downregulation cooperates with anti-PD-1 therapy to reduce the presence of suppressor Tregs in the tumor microenvironment.

Concurrent with this, anti-PD-1 treatment in dLCK-CRE mice also led to a significant reduction in both the frequency and expression of the inhibitory receptor TIM3 on CD44+CD4+ TILs, as demonstrated by flow cytometry analysis. This was evident in the FACS plots (Fig. 6C), percentage of TIM3+ cells (Fig. 6D), and MFI measurements (Fig. 6E).

Considering these findings, we assessed whether the rejection of tumors was dependent on CD4+ T-cells (Fig. 6F). The greater relative loss of Tregs in WT with anti-PD-1 therapy might reflect a positive effect with CD4+ T-cell depletion, while the more potent loss of Tregs and a relative increase in the presence of T-helper cells might be predicted to reflect a greater dependency of GSK-3 KD T-cells helper function so that the depletion of CD4+ cells in GSK-3KD will mostly have a negative effect.

To this end, anti-CD4 was injected at various time to deplete CD4+ T-cells prior to and during anti-PD-1 therapy. Interestingly, anti-PD-1 was able to reject the B16-F10 R1 tumors normally in WT mice (Fig. 6F). This was seen in terms of tumor volume (Fig. 6F) and tumor weight (Fig. 6G). These observations indicated that the loss of CD4+ T-cells allowed anti-PD-1 to reject tumors in a manner not observed when CD4+ T-cells were present, suggestive of a role for suppressor CD4 T-cells in limiting tumor rejection.

Conversely, in dLCK-CRE mice with normally heightened responses, the absence of CD4+ T-cells precluded anti-PD-1-mediated tumor rejection (Fig. 6F,G). This observation was corroborated by the analysis of CD8+ TILs. While anti-PD-1 treatment augmented the percentage (Fig. 6H) and absolute number (Fig. 6I) of CD8+ TILs in wild-type (WT) mice, no such increase was observed in CD4 depleted GSK-3 knockdown mice. The absence of CD4+ T cells in FACs plots confirmed the efficacy of anti-CD4 depletion. These findings suggest that

CD4+ T-cell help is crucial for effective anti-PD-1 immunotherapy in the context of reduced GSK-3 activity. This dependence may stem from the role of CD4+ T-cells in priming CD8+ T-cells for optimal tumor-killing capabilities. Further, the enhanced expression of GZMs observed in GSK-3 KD mice (Fig. 5) was abrogated in the absence of CD4+ T cells (Fig. 6J). These data indicate that GSK-3 signaling modulates the requirement for CD4+ T-cell help during tumor rejection. Reduced GSK-3 expression establishes a reliance on CD4+ T-cell help that is not evident under normal physiological conditions.

Discussion

Despite its importance in T-cell signaling, the full role of GSK-3 in immune function has yet to be explored. Here, we show for the first time that GSK-3 controls CD4-CD8 T-cell crosstalk in synergy with anti-PD-1 blockade, leading to the generation of a GZM-enriched population of super-armed CD8+ effectors in immunotherapy. The genetic knockdown of GSK-3 increased memory TCF-1+ T-cells with reduced overall exhaustion for more potent anti-viral and tumor immunity. Further, GSK-3 knockdown and inhibition were found to license anti-PD-1 to overcome tumor resistance in a process that down-regulated CD4+ Tregs while increasing the presence of effector-memory CD8+ T-cells. This synergy resulted in the generation of super-armed killer T-cells expressing an unprecedented 7/9 cytolytic granzymes (GZMs K, G, E, F, D, B, C). Importantly, reduced GSK-3 expression established a reliance on CD4+ T-cell help that is not evident under normal physiological conditions. Our findings offer a novel therapeutic strategy for cancer immunotherapy, with the potential to improve treatment outcomes by optimizing T-cell responses and CD4-CD8 T-cell crosstalk needed to increase GZM expression.

One central finding was that GSK-3 KD and inhibition licensed anti-PD-1 to overcome tumor resistance dependent on CD4 and CD8 T-cell cooperativity. An ability to overcome melanoma tumors resistant to ICB immunotherapy has significant relevance in the current era, where 40-50% of patients remain unresponsive. Our B16 F10 R1 was completely resistant to all tested doses of anti-PD-1 and GSK-3 inactivation monotherapy. The loss of highly suppressive FOXP3hi CD25+ CD73+ Tregs combined with increased numbers of effector memory TILs would be expected to complement each other, where decreased suppression promotes cytolytic CD8 effectors [90, 91].

Further, with a cutoff criterion of a 2-fold increase and a p-value cutoff of 0.001, GSK-3 licensing with anti-PD-1 induced 37 genes, among which we observed the induction of the cytolytic pore protein, perforin[92] and remarkable 7/9 granzymes. To our knowledge, this preferential upregulation of a group of killer proteins is unprecedented and indicative of the 'super-arming' of cytolytic T cells, enhancing their capacity for tumor destruction. The granzymes/serine proteases included the well-known GZMB as well as less well known granzymes such as GZMK, GZMG, GZME, GZMF, GZMD, and GZMC [82]. GZMF high expressing cells are distinct from GZMA and B expressing cells in their elimination of cancer cells [93]. Further, GZMC and GZMK employ a different mechanism of killing via a caspase-

independent pathway[32]. These findings indicate GSK-3-anti-PD-1 synergy induces different pathways of killing employing different cells and mechanisms. To confirm an involvement of lesser-known GZMs, we showed that the downregulation of GZMD and GZMF in OT-1 T-cells reduced the killing of EL4 tumor targets. Collectively, these data suggest that combination therapy super-arms CD8+ T-cells to become more effective in tumor killing.

Equally important, the upregulation of these mechanisms was critically dependent on GSK-3 regulation of CD4 help for CD8 T-cells. Helper CD4+ T-cells, provide positive signals needed to activate CD8+ T-cells, while CD4+ FoxP3+ T-cells suppress T-cell responses[57]. In the absence of CD4 T-cell help, CD8 T-cells become dysfunctional, losing their cytotoxic capacity for viral control[4, 5, 6]. Under conditions of CD4+ T-cell depletion, anti-PD-1 was more potent in cooperating with WT T-cells to limit tumor growth. Firstly, we observed that anti-PD-1 has different effects on the composition of CD4-positive TILs. In WT mice, an increase in Treg TILs was seen, while in GSK-3 KD mice, the opposite result was seen: a decrease in Tregs and an increase in FoxP3-negative helper T-cells. The depletion of CD4+ T-cells and its co-depletion of Tregs allowed anti-PD-1 to now reject the ICB-resistant B16 F10 R1 tumor in WT mice. This indicated that the increase in Tregs was indeed limiting the potency of checkpoint blockade.

On the other hand, the depletion of CD4+ T-cells in the GSK-3 KD mice caused the opposite result, namely, it prevented CD8+ T-cells from entering and destroying the tumor as well as preventing the induction of the various GZMs induced by combination therapy. This finding was most compatible with a model where the increase in the presence of T-helper cells in response to anti-PD-1 in GSK-3 KD mice was providing essential help to CD8+ T-cells to become super-armed to kill the tumor cells. The exact mechanism by which this help is provided will require further work.

One contributing factor not yet reported is that the reduction in GSK-3 caused T-cells to be more reliant on glycolysis relative to oxidative phosphorylation for their energy requirements. The effect on extracellular acidification rate (ECAR) was more striking than on the oxygen consumption rate (OCR) with a lower OCR/ECAR ratio. This reliance on glucose uptake was also evident with the greater glucose uptake and GLUT-1 expression on GSK-3 KD cells, where this effect was most evident in GP33+ CD8+ memory precursor effector cells (MPECs). This observation, combined with the greater cell division evident in MPECs, as seen with Ki67 expression (data not showed), is consistent with the shift in T-cells from the primarily use of oxidative phosphorylation to glycolysis upon activation[94],[95]. In addition, stem-like progenitor T-

cells primarily utilize glycolysis to generate ATP[96]. Although not reported before for T-cells, B-cell responses to the co-stimulatory receptor CD40 also engage glycolysis[97].

Lastly, our findings showed that GSK-3 KD favored the generation of TCF1+ stem-like progenitor cells. Studies have shown the requirement for stem-like T-cells for an anti-tumor response in checkpoint blockade[24, 25, 26]. Although the effects of non-specific chemical inhibitors have been associated with T-cell progenitors[98], to date there have been no reports of an analysis of genetically knocked down mice in CD4+ and CD8+ T-cells. A selective KO in CD8+ T-cells showed an increase in non-exhausted T-cells but failed to establish a link to TCF-1 and the generation of TCF-1+ progenitor T-cells[99]. This feature was amplified in LCMV Cl13 infection, showing a continued increase in both central and effector memory T-cells as well as a preferential increase in the presence of MPECs relative to SLECs. Surprisingly, the same subset showed an increase in the expression of the cell cycle marker Ki67 in GSK-3 KD but not wild-type mice (data not showed). Further, the same subset showed an increase in the expression of GLUT-1 and an increase in glucose uptake. In this way, MPECs play a key role in developing long-lasting immunological memory to respond to future infections[100, 101]. Our observations place GSK-3 upstream in the control of the generation of TCF-1+ stem-like memory T-cells[102, 103].

The findings in this paper and previously[57, 58, 59, 62, 63] by several groups showed that the inactivation of GSK-3 generated enhanced anti-tumor immunity. In fact, clinical trials are now underway using GSK-3 inhibitors such as Elraglusib to treat prostate cancer[64, 65]. These studies contrast with the findings of another GSK-3 KO showing increased tumor growth[99]. Several factors may explain these divergent outcomes. The paper is a GZMB driven KO with unclear consequences for thymic development[104, 105, 106] and where B-cell, Treg, mast and neutrophils express GZMB. Tregs have been reported to mediate suppression via the induction of death by granzyme B-dependent killing[107]. This might reflect the role of GSK-3 in other populations of interacting cells. In addition, T-cell exhaustion was assessed at day 7 following LCMV infection, well before exhaustion is seen, Overall, our findings underscore the importance of the serine/threonine kinase GSK-3 in governing the nature of the immune response in checkpoint blockade, both in terms of its control of the cooperation between CD4 and CD8 T-cells and enhanced GZM expression in anti-PD-1 therapy.

Methods

Ethic approval

Animal experiments were approved by the Animal Care Use and Review Committee of Center Research -Hospital Maisonneuve Rosemont (CR-HMR) (ethical approval no 2021-2516, 2023-3032 and 2024-3547) from University of Montreal. For mouse tumor experiments, all tumor sizes/burdens were permitted by the CR-HMR of Montreal University. Maximal tumor burden permitted by the CR-HMR (1.5 cm3) was not exceeded in this study.

Key resources

A complete list of the reagents and antibodies used in this manuscript can be found in supplementary table S1.

Animals

To obtain GSK-3$\alpha^{flox/flox}$ $\beta^{flox/flox}$ mice, GSK-3$\alpha^{flox/flox}$ GSK-3 $\beta^{flox/flox}$ were crossed. In a second time, GSK-3$\alpha^{flox/flox}$ $\beta^{flox/flox}$ mice were crossed with or *dLCK-Cre* (B6.Cg-Tg$^{(Lck\text{-}icre)3779Nik/J}$) mice from the Jackson laboratory to inactivate both apha and beta isoform of GSK-3 in progenitor T cells and mature T cells respectively. All mice were housed in an animal facility with a 12 h light/12 h dark cycle and had free access to food and water throughout the study period. The study is compliant with all of the relevant ethical regulations regarding animal research. Sex was not considered in the study design and analysis because this study was not designed to detect sex differences.

Viral infections

LCMV Armstrong and clone 13 were grown in BHK cells and titrated using plaque assay on VERO cells. Recipient mice were infected either intraperitoneally (i.p.) with LCMV Armstrong ($2x10^5$ plaque forming units [PFU]) or intravenously (i.v.) with LCMV clone13 ($2x10^5$ PFU). After infection, mice were respectively sacrificed at d7 and d30.

Cell lines

B16F10 tumor cells were maintained in DMEM supplemented with 10% FCS, 1% L-glut and 1% Pen/Strep. Tumor cells ($2x10^5$) cultured for less than two weeks were implanted subcutaneously in the flank of recipient mice using 29G1/2 syringes. Tumor size was

monitored using a manual caliper and tumors were excised before exceeding the volume permitted by CR-HMR ethic committee.

Mice injection and CD4+ T-cell depletion

Anti-PD-1 antibodies from (Leinco) and SB415286 (Selleckchem) were diluted at 1mg/ml and 200ug were IP injected in mice each 2 days from d6 post-implantation until tumor extraction on day 16. For TCD4 cell depletion, mice were IP injected with 300 ug of anti-CD4 (Leinco) one day before tumor implantation, d7 and d14 post implantation.

Cell preparation and *ex-vivo* activation

Spleen were taken from 8- to 16-week-old mice and pressed in a 6 wells plate containing 2ml of red blood lysis buffer 2 more ml were added and then incubated 5min at RT. Lysis was stopped with 20ml of PBS and the solution was filtered on a 70µm membrane and then centrifuged 5min at 350g. Pellets from spleen cells were resuspended in 1ml of PBS/2mM EDTA + 2% FBS (Facs buffer) and alive cells were counted on a Neubauer counting chamber with Trypan blue. T cells were isolated with magnetic kit (Stemcell Technologies), and 2.10^6 cells were seed in 1ml of activation media (RPMI+L-glutamine+ FBS[10%]+ HPES[1M]+β-mercaptoetanol [0,1%]) in a 48 wells pate media and activated with 1ug/ml with anti-CD3e for 24h at 37°C.

Glucose uptake

Cells from spleen were isolated as previously described and activated with 1ug/ml of anti-CD3e for 48h at 37°C. Then, cells were incubated with 2-NBDG (ThermoFisher # N13195) diluted 1/1000 in PBS at 37°C for 1h.

Seahorse

The Seahorse XF24 metabolite analyzer was used to measure oxygen consumption and proton production. T cells were isolated and activated as described in the specific section on Cell-Tak coated Seahorse cell culture plates. Cells were incubated for 1.5 h in Seahorse assay medium supplemented with 10 mM glucose and 1 mM sodium pyruvate before measurement. Mito Stress assay kit (Rot/AA [0,5um] ; 2-NBDG [50um]) and glycolytic rate assay kit (oligomycine [1,5um]; FCCP [2um] ;ROT/AA [0,5um]) from Agilent were used to examine different parameters of glycolysis and respiration.

Reagents and antibodies

A complete list of the reagents and antibodies used in this manuscript can be found in supplementary table S1.

Cell preparation, facs staining and immunophenotyping

All organs were taken from from 8- to 16-week-old mice. inguinal lymph nodes (LN) and thymus were mechanically disrupted onto a 70um strainer using the plunger of a 5mL syringe. Stainer was wash with 5ml of Facs buffer. Tumors were smashed on 70 um strainers in RPMI on ice. Tumor lysate was spined down at 350g for 5min and resuspended in PBS. PBS containing tumor lysate was add to lymphocytes separation medium (Corning) and TILs were separated and isolated after centrifugation at 2000 rpm for 20 min at RT. Isolated cells from spleen, LN, thymus, and tumor blocked with 100µl of PBS/10mM EDTA + FBS 5% + 2,5 ng/ml purified rat anti-mouse CD16/CD32 (BD Biosciences #553141) 20min at 4°C. Cells were then centrifuged 5min at 350g and stained with primary antibodies (Table in supplementary figure) for 30min at 4°C. Each mix was supplemented by 1/1000 Fixable Viability Dye eFluor™ 780. Cells were fixed with 2% PAF 15min at 4°C, washed 2 times in PBS/10mM EDTA +FBS 2% and then nuclear permeabilized with FOXP3 kit (Biolegend) for 30 min at 4°C. Cells were stained with antibodies targeting intracellular protein, diluted in permeabilization buffer for 50min at RT and washed 2 times in PBS/10mM EDTA +FBS 2%. Cells suspensions were analyzed with LSRFortessa (BD biosciences). Mean fluorescence intensity (MFI) of specific markers was quantified on T cell subpopulations using FlowJo. Results were analyzed using FlowJo (Tree Star, Ashland, USA).

Cell lysis, and Immunoblotting

CD8+ T cells were isolated (Stemcell Technologies). Cell lysates were prepared by resuspension of spleen-purified CD8+ T cells in 1% Triton X-100 lysis buffer, followed by a 30-min incubation on ice. Lysates were centrifuged at 14,000 rpm for 30 min at 4°C and the nuclear-free supernatants were subjected to SDS-PAGE on a 10 % polyacrylamide gel. Proteins from the gel were electroblotted onto nitrocellulose membranes at 100V for 75 min, followed by 1 h of blocking with 3% BSA in TBST at RT. The nitrocellulose membranes were then incubated in the presence of the indicated primary Abs, followed by incubation with HRP-conjugated secondary Abs. Immunoreactive protein bands were visualized using an ECL reagent and autoradiography. Whenever required, nitrocellulose membranes were

stripped by incubation in stripping buffer for 20 min at RT, followed by 1 h incubation with blocking buffer (3% BSA in TBST).

Mass cytometry (CyTOF)

Mass cytometry (CyTOF) analysis was performed at the McGill University CyTOF facility following standardized protocols. Single-cell suspensions (3×10^6 cells) were stained with 5μM Cell-ID™ Cisplatin (Fluidigm, San Francisco, CA) for viability assessment, followed by32quenching with MaxPar® Cell Staining Buffer at a 5:1 volume ratio. Following centrifugation (300g, 5 min, 4°C), cells were resuspended in 50 μL buffer and incubated with human Fc receptor blocking solution (5 μL; BioLegend, San Diego, CA) for 10 minutes at room temperature. Surface marker staining was performed using 50 μL of pre-titrated metal conjugated antibody cocktail for 30 minutes (detailed panel composition in Reference 20).After washing, cellular DNA was labeled overnight at 4°C using 1 mL intercalation solution containing 125 nM MaxPar® Intercalator-Ir in MaxPar® Fix and Perm Buffer. Prior to data acquisition, cells were washed with MaxPar® Water, resuspended with EQ™ Four Element Calibration Beads, and analyzed on a Helios™ CyTOF II mass cytometer. A minimum of 100,000 viable single cells were acquired per sample at an event rate of 300-500 events/second. Analysis was performed on using antibodies against CD45, TCR-beta as indicated in Figure 4A.

Mass cytometry data analysis

Mass cytometry data analysis was performed using the Cytobank platform (Cytobank Inc., Mountain View, CA) following previously established protocols94, 95. All samples underwent simultaneous normalization and analysis to minimize technical variation and account for signal drift during extended acquisition periods. A standardized high-level gating strategy was implemented across all CyTOF files, incorporating sequential gates for event length, bead exclusion, cell viability, and DNA content. For comprehensive analysis, individual sample files were concatenated into a single dataset, from which population-specific data were subsequently extracted and separated into individual files for comparative analyses. Dimensional reduction was performed using t-Distribution Stochastic Neighbor Embedding (tSNE) analysis, which generated a two-dimensional representation (tSNE1 versus tSNE2) of the high-dimensional data by preserving local phenotypic relationships between cells,

enabling visualization and identification of distinct cell populations based on their marker expression profiles.

Sample preparation for RNaseq and RNA profilling

Tumor was prepared as previously described and CD8+ TILs were isolated (Stemcell Technologies) RNA was isolated using the miRNeasy Mini Kit (Qiagen), and the mRNA was purified from 1ug of total RNA using the Dynabeads mRNA DIRECT Micro Kit (Thermo Fisher Scientific). The reverse transcription used SuperScript VILO cDNA Synthesis kit (Thermo Fisher Scientific). The whole transcriptome libraries were prepared using the Ion Total RNA-Seq Kit version 2 Kit (Thermo Fisher Scientific). The yield and size distribution of the amplified libraries were assessed with Agilent Bioanalyzer using Ion AmpliSeq transcriptome Mouse gene expression Kit (Thermo Fisher Scientific). Sequencing was performed on an Ion Proton Instrument (Ion Torrent, Thermo Fisher Scientific). RNA-sequencing (RNA-seq) analysis was done using the Torrent Suite software version 5.4.0 and the RNASeqAnalysis plugin (Thermo Fisher Scientific) on the mouse reference genome mm10 using STAR. Gene level expression is calculated using HTSeq and Picard to report raw read counts and FPKM (fragment per kilobase of transcript per million).

Killing assay

EL4 cells (Target) were cultivated in RPMI + 10%FBS and incubated at RT for 25 min with Tag-it 1/1000.Then, EL4 cells were pulsed with 1 µg/ml of OVA peptide at 37°C for 1 hour. OT1 splenocytes (Effector) were isolated as previously described and activated with Anti-CD28 2ug/mL + IL-2 5ng/mL and anti-CD3e 2ug/mL in activation media for 1 day at 37°C. Effector cell were electroporated with 125nM of GZM siRNA or Ctrl siRNA and cultivated overnight in RPMI+20% FBS+2%L-Glutamine+anti-CD3 (2ug/mL) and anti-CD28 (2ug/mL) + IL2 (5ng/mL). Next day, cells were spin down at 300g for 5min, resuspended at the concentration of 10^6/mL and cultivated for 24h in activated media + IL2 (50IU/mL). Next day 25000 of target cell were colcultured for 6 days in activation media with 250000 effector electroporated cells; Ration (E:T)=10:1 and dead percentage of target cell (Tag-it +) were analysed in facs using a viability dye.

Statistical analysis

Respect of the assumptions of normal distribution of residuals and homoscedasticity was verified, and data were presented as mean + SEM as well as individual values, unless otherwise indicated. Data from independent experiments were pooled for analysis in each data panel, unless otherwise indicated. Statistical analyses were performed using Prism 8 (GraphPad Software). Two-ways unpaired *t* test was performed unless otherwise indicated in the figure legends. We considered a P-value lower than 0,05 as significant. N.S.: $P>0,05$; *: $P<0,05$; **: $P<0,01$; ***: $P<0,001$; ****$P<0,0001$.

Reporting summary

Further information on research design is available in the Nature Portfolio Reporting Summary linked to this article

Data availability

N.A.

Code availability

N.A.

References

1. Kalia, V., Sarkar, S. & Ahmed, R. Fine-tuning CD4+ central memory T cell heterogeneity by strength of stimulation. *European journal of immunology* **38**, 15-19 (2008).

2. Topchyan, P., Lin, S. & Cui, W. The Role of CD4 T Cell Help in CD8 T Cell Differentiation and Function During Chronic Infection and Cancer. *Immune Netw* **23**, e41 (2023).

3. Laidlaw, B.J., Craft, J.E. & Kaech, S.M. The multifaceted role of CD4(+) T cells in CD8(+) T cell memory. *Nat Rev Immunol* **16**, 102-111 (2016).

4. Zajac, A.J. *et al.* Viral immune evasion due to persistence of activated T cells without effector function. *J Exp Med* **188**, 2205-2213 (1998).

5. Aubert, R.D. *et al.* Antigen-specific CD4 T-cell help rescues exhausted CD8 T cells during chronic viral infection. *Proceedings of the National Academy of Sciences of the United States of America* **108**, 21182-21187 (2011).

6. Battegay, M., Moskophidis, D., Rahemtulla, A., Hengartner, H., Mak, T.W. & Zinkernagel, R.M. Enhanced establishment of a virus carrier state in adult CD4+ T-cell-deficient mice. *J Virol* **68**, 4700-4704 (1994).

7. Mikami, N. & Sakaguchi, S. Regulatory T cells in autoimmune kidney diseases and transplantation. *Nat Rev Nephrol* **19**, 544-557 (2023).

8. Tay, C., Tanaka, A. & Sakaguchi, S. Tumor-infiltrating regulatory T cells as targets of cancer immunotherapy. *Cancer Cell* **41**, 450-465 (2023).

9. Wood, K.J. & Sakaguchi, S. Regulatory T cells in transplantation tolerance. *Nat Rev Immunol* **3**, 199-210 (2003).

10. McLane, L.M., Abdel-Hakeem, M.S. & Wherry, E.J. CD8 T cell exhaustion during chronic viral infection and cancer. *Annu Rev Immunol* (2019).

11. Hudson, W.H. *et al.* Proliferating Transitory T Cells with an Effector-like Transcriptional Signature Emerge from PD-1(+) Stem-like CD8(+) T Cells during Chronic Infection. *Immunity* **51**, 1043-1058 e1044 (2019).

12. Chen, Z. *et al.* TCF-1-Centered Transcriptional Network Drives an Effector versus Exhausted CD8 T Cell-Fate Decision. *Immunity* **51**, 840-855 e845 (2019).

13. Baumeister, S.H., Freeman, G.J., Dranoff, G. & Sharpe, A.H. Coinhibitory Pathways in Immunotherapy for Cancer. *Annu Rev Immunol* **34**, 539-573 (2016).

14. Sharma, P. *et al.* The Next Decade of Immune Checkpoint Therapy. *Cancer Discov* **11**, 838-857 (2021).

15. Curran, M.A., Montalvo, W., Yagita, H. & Allison, J.P. PD-1 and CTLA-4 combination blockade expands infiltrating T cells and reduces regulatory T and myeloid cells within B16 melanoma tumors. *Proc Natl Acad Sci U S A* **107**, 4275-4280 (2010).

16. Ott, P.A., Hodi, F.S. & Robert, C. CTLA-4 and PD-1/PD-L1 blockade: new immunotherapeutic modalities with durable clinical benefit in melanoma patients. *Clinical cancer research : an official journal of the American Association for Cancer Research* **19**, 5300-5309 (2013).

17. Nguyen, L.T. & Ohashi, P.S. Clinical blockade of PD1 and LAG3--potential mechanisms of action. *Nat Rev Immunol* **15**, 45-56 (2015).

18. Rudd, C.E., Krueger, J. & Taylor, A. Exploiting intracellular pathways of co-receptor expression in the future of immunotherapy. *Nat Rev Immunol* **in press** (2019).

19. Ben Saad, E., Oroya, A., Anto, N.P., Bachais, M. & Rudd, C.E. PD-1 endocytosis unleashes the cytolytic potential of checkpoint blockade in tumor immunity. *Cell Rep* **43**, 114907 (2024).

20. Lin, W.W. *et al.* CD8(+) T Lymphocyte Self-Renewal during Effector Cell Determination. *Cell Rep* **17**, 1773-1782 (2016).

21. Pais Ferreira, D. *et al.* Central memory CD8(+) T cells derive from stem-like Tcf7(hi) effector cells in the absence of cytotoxic differentiation. *Immunity* **53**, 985-1000 e1011 (2020).

22. Gullicksrud, J.A. *et al.* Differential Requirements for Tcf1 Long Isoforms in CD8(+) and CD4(+) T Cell Responses to Acute Viral Infection. *J Immunol* **199**, 911-919 (2017).

23. Lin, W.H. *et al.* Asymmetric PI3K Signaling Driving Developmental and Regenerative Cell Fate Bifurcation. *Cell Rep* **13**, 2203-2218 (2015).

24. Siddiqui, I. *et al.* Intratumoral Tcf1(+)PD-1(+)CD8(+) T cells with stem-like properties promote tumor control in response to vaccination and checkpoint blockade immunotherapy. *Immunity* **50**, 195-211 e110 (2019).

25. Sade-Feldman, M. *et al.* Resistance to checkpoint blockade therapy through inactivation of antigen presentation. *Nat Commun* **8**, 1136 (2017).

26. Miller, B.C. *et al.* Subsets of exhausted CD8(+) T cells differentially mediate tumor control and respond to checkpoint blockade. *Nat Immunol* **20**, 326-336 (2019).

27. Barry, M. & Bleackley, R.C. Cytotoxic T lymphocytes: all roads lead to death. *Nat Rev Immunol* **2**, 401-409 (2002).

28. Cullen, S.P., Brunet, M. & Martin, S.J. Granzymes in cancer and immunity. *Cell Death Differ* **17**, 616-623 (2010).

29. Hay, Z.L.Z. & Slansky, J.E. Granzymes: The Molecular Executors of Immune-Mediated Cytotoxicity. *Int J Mol Sci* **23** (2022).

30. <Beresford, P.J. 1999.pdf>.

31. Metkar, S.S. *et al.* Human and mouse granzyme A induce a proinflammatory cytokine response. *Immunity* **29**, 720-733 (2008).

32. Johnson, H., Scorrano, L., Korsmeyer, S.J. & Ley, T.J. Cell death induced by granzyme C. *Blood* **101**, 3093-3101 (2003).

33. Rudd, C.E. Adaptors and molecular scaffolds in immune cell signaling. *Cell* **96**, 5-8 (1999).

34. Wang, H. & Rudd, C.E. SKAP-55, SKAP-55-related and ADAP adaptors modulate integrin-mediated immune-cell adhesion. *Trends Cell Biol* **18**, 486-493 (2008).

35. Finlay, D. & Cantrell, D.A. Metabolism, migration and memory in cytotoxic T cells. *Nature reviews. Immunology* **11**, 109-117 (2011).

36. Rudd, C.E. How the Discovery of the CD4/CD8-p56(lck) Complexes Changed Immunology and Immunotherapy. *Front Cell Dev Biol* **9**, 626095 (2021).

37. Samelson, L.E. Signal transduction mediated by the T cell antigen receptor: the role of adapter proteins. *Annu Rev Immunol* **20**, 371-394 (2002).

38. Barber, E.K., Dasgupta, J.D., Schlossman, S.F., Trevillyan, J.M. & Rudd, C.E. The CD4 and CD8 antigens are coupled to a protein-tyrosine kinase (p56lck) that phosphorylates the CD3 complex. *Proc Natl Acad Sci U S A* **86**, 3277-3281 (1989).

39. Chan, A.C., Iwashima, M., Turck, C.W. & Weiss, A. ZAP-70: a 70 kd protein-tyrosine kinase that associates with the TCR zeta chain. *Cell* **71**, 649-662 (1992).

40. Rudd, C.E. & Raab, M. Independent CD28 signaling via VAV and SLP-76: a model for in trans costimulation. *Immunol Rev* **192**, 32-41 (2003).

41. Crespo, A.R., Luna, S.G., Moes, B., Rodriguez, A. & Rudd, C.E. The many faceted role of glycogen synthase kinase-3 (GSK-3) in T cells and cancer immunotherapy. *J Cancer Biol* **5**, 11-16 (2024).

42. Woodgett, J.R. Judging a protein by more than its name: GSK-3. *Science's STKE : signal transduction knowledge environment* **2001**, re12 (2001).

43. Embi, N., Rylatt, D.B. & Cohen, P. Glycogen synthase kinase-3 from rabbit skeletal muscle. Separation from cyclic-AMP-dependent protein kinase and phosphorylase kinase. *European journal of biochemistry / FEBS* **107**, 519-527 (1980).

44. Beurel, E., Grieco, S.F. & Jope, R.S. Glycogen synthase kinase-3 (GSK3): regulation, actions, and diseases. *Pharmacol Ther* **148**, 114-131 (2015).

45. Gounari, F. & Khazaie, K. TCF-1: a maverick in T cell development and function. *Nat Immunol* **23**, 671-678 (2022).

46. Zhao, P., Sun, L. & Zhao, C. TCF1/LEF1 triggers Wnt-dependent chemokine/cytokine-induced inflammation and cadherin pathways to drive T-ALL cell migration. *Biochem Biophys Rep* **34**, 101457 (2023).

47. Woodgett, J.R. Molecular cloning and expression of glycogen synthase kinase-3/factor A. *EMBO J* **9**, 2431-2438 (1990).

48. Doble, B.W. & Woodgett, J.R. GSK-3: tricks of the trade for a multi-tasking kinase. *J Cell Sci* **116**, 1175-1186 (2003).

49. Rayasam, G.V., Tulasi, V.K., Sodhi, R., Davis, J.A. & Ray, A. Glycogen synthase kinase 3: more than a namesake. *Br J Pharmacol* **156**, 885-898 (2009).

50. Frame, S. & Cohen, P. GSK3 takes centre stage more than 20 years after its discovery. *Biochem J* **359**, 1-16 (2001).

51. Hughes, K., Nikolakaki, E., Plyte, S.E., Totty, N.F. & Woodgett, J.R. Modulation of the glycogen synthase kinase-3 family by tyrosine phosphorylation. *Embo J* **12**, 803-808 (1993).

52. Woodgett, J.R. Molecular cloning and expression of glycogen synthase kinase-3/factor A. *Embo J* **9**, 2431-2438 (1990).

53. Eldar-Finkelman, H. & Martinez, A. GSK-3 inhibitors: preclinical and focus on CNS. *Front Mol Neurosci*, doi: 10.3389/fnmol.2011.00032 (2011).

54. McManus, E.J. *et al.* Role that phosphorylation of GSK3 plays in insulin and Wnt signalling defined by knockin analysis. *EMBO J* **24**, 1571-1583 (2005).

55. Phiel, C.J., Wilson, C.A., Lee, V.M. & Klein, P.S. GSK-3alpha regulates production of Alzheimer's disease amyloid-beta peptides. *Nature* **423**, 435-439 (2003).

56. Martin, M., Rehani, K., Jope, R.S. & Michalek, S.M. Toll-like receptor-mediated cytokine production is differentially regulated by glycogen synthase kinase 3. *Nat Immunol* **6**, 777-784 (2005).

57. Taylor, A., Harker, J.A., Chanthong, K., Stevenson, P.G., Zuniga, E.I. & Rudd, C.E. Glycogen synthase kinase 3 inactivation drives T-bet-mediated downregulation of co-receptor PD-1 to enhance CD8(+) cytolytic T cell responses. *Immunity* **44**, 274-286 (2016).

58. Rudd, C.E., Chanthong, K. & Taylor, A. Small Molecule Inhibition of GSK-3 Specifically Inhibits the Transcription of Inhibitory Co-receptor LAG-3 for Enhanced Anti-tumor Immunity. *Cell Rep* **30**, 2075-2082 e2074 (2020).

59. Taylor, A., Rothstein, D. & Rudd, C.E. Small-molecule inhibition of PD-1 transcription Is an effective alternative to antibody blockade in cancer therapy. *Cancer Res* **78**, 706-717 (2018).

60. Krueger, J. & Rudd, C.E. Two Strings in One Bow: PD-1 Negatively Regulates via Co-receptor CD28 on T Cells. *Immunity* **46**, 529-531 (2017).

61. Steele, L. *et al.* Non-redundant activity of GSK-3alpha and GSK-3beta in T cell-mediated tumor rejection. *iScience* **24**, 102555 (2021).

62. Taylor, A. & Rudd, C.E. Glycogen synthase kinase 3 (GSK-3) controls T-cell motility and interactions with antigen presenting cells. *BMC Res Notes* **13**, 163 (2020).

63. Taylor, A. & Rudd, C.E. Glycogen Synthase Kinase 3 Inactivation Compensates for the Lack of CD28 in the Priming of CD8(+) Cytotoxic T-Cells: Implications for anti-PD-1 Immunotherapy. *Front Immunol* **8**, 1653 (2017).

64. Huntington, K.E. *et al.* GSK-3 Inhibitor Elraglusib Enhances Tumor-Infiltrating Immune Cell Activation in Tumor Biopsies and Synergizes with Anti-PD-L1 in a Murine Model of Colorectal Cancer. *Int J Mol Sci* **24** (2023).

65. Shaw, G., Cavalcante, L., Giles, F.J. & Taylor, A. Elraglusib (9-ING-41), a selective small-molecule inhibitor of glycogen synthase kinase-3 beta, reduces expression of immune checkpoint molecules PD-1, TIGIT and LAG-3 and enhances CD8(+) T cell cytolytic killing of melanoma cells. *J Hematol Oncol* **15**, 134 (2022).

66. Van Oers, N.S. *et al.* Disruption of CD8-dependent negative and positive selection of thymocytes is correlated with a decreased association between CD8 and the protein tyrosine kinase, p56lck. *Eur J Immunol* **22**, 735-743 (1992).

67. Barber, D.L. *et al.* Restoring function in exhausted CD8 T cells during chronic viral infection. *Nature* **439**, 682-687 (2006).

68. Kim, H.D. *et al.* Implication of CD69(+) CD103(+) tissue-resident-like CD8(+) T cells as a potential immunotherapeutic target for cholangiocarcinoma. *Liver Int* **41**, 764-776 (2021).

69. Wherry, E.J. T cell exhaustion. *Nature immunology* **12**, 492-499 (2011).

70. Abadie, K. *et al.* Reversible, tunable epigenetic silencing of TCF1 generates flexibility in the T cell memory decision. *Immunity* **57**, 271-286 e213 (2024).

71. Sakuishi, K., Apetoh, L., Sullivan, J.M., Blazar, B.R., Kuchroo, V.K. & Anderson, A.C. Targeting Tim-3 and PD-1 pathways to reverse T cell exhaustion and restore anti-tumor immunity. *The Journal of experimental medicine* **207**, 2187-2194 (2010).

72. Ke Xu, N.Y., Min Peng, Efstathios G. Stamatiades, Amy Shyu1,4, Peng Li1, Xian Zhang1, Mytrang H. Do1,2, Zhaoquan Wang1,2, Kristelle J. Capistrano1, Chun Chou1, Andrew G. Levine1,2, Alexander Y. Rudensky1,2,5, Ming O. Li1,2†. Glycolysis fuels phosphoinositide 3-kinase signaling to bolster T cell immunity. *Science* (2021).

73. Wu, M. *et al.* Glucose metabolism and function of CD4(+) Tregs are regulated by the TLR8/mTOR signal in an environment of SKOV3 cell growth. *Cancer Med* **12**, 16310-16322 (2023).

74. Sicheng Fu1, S.Z., Chenxi Tian, Shiyu Bai1, Jiqian Zhang, Chonglun Zhan, Di Xie, Lu Wang, Zonghong Li. Immunometabolism regulates TCR recycling and iNKT cell functions. *Sci.signal* (2019).

75. Palmer, C.S. *et al.* Regulators of Glucose Metabolism in CD4(+) and CD8(+) T Cells. *Int Rev Immunol* **35**, 477-488 (2016).

76. Frauwirth, K.A. *et al.* The CD28 signaling pathway regulates glucose metabolism. *Immunity* **16**, 769-777 (2002).

77. Macintyre, A.N. *et al.* The glucose transporter Glut1 is selectively essential for CD4 T cell activation and effector function. *Cell Metab* **20**, 61-72 (2014).

78. Gantt, K.R., Cherry, J., Richardson, M., Karschner, V., Atasoy, U. & Pekala, P.H. The regulation of glucose transporter (GLUT1) expression by the RNA binding protein HuR. *J Cell Biochem* **99**, 565-574 (2006).

79. Wei, S.C. *et al.* Distinct cellular mechanisms underlie anti-CTLA-4 and anti-PD-1 checkpoint blockade. *Cell* **170**, 1120-1133 e1117 (2017).

80. Sakaguchi, S., Yamaguchi, T., Nomura, T. & Ono, M. Regulatory T cells and immune tolerance. *Cell* **133**, 775-787 (2008).

81. Allard, D., Chrobak, P., Allard, B., Messaoudi, N. & Stagg, J. Targeting the CD73-adenosine axis in immuno-oncology. *Immunol Lett* **205**, 31-39 (2019).

82. Russell, J.H. & Ley, T.J. Lymphocyte-mediated cytotoxicity. *Annu Rev Immunol* **20**, 323-370 (2002).

83. Osinska, I., Popko, K. & Demkow, U. Perforin: an important player in immune response. *Cent Eur J Immunol* **39**, 109-115 (2014).

84. Kurschus, F.C. & Jenne, D.E. Delivery and therapeutic potential of human granzyme B. *Immunol Rev* **235**, 159-171 (2010).

85. Smyth, M.J., O'Connor, M.D. & Trapani, J.A. Granzymes: a variety of serine protease specificities encoded by genetically distinct subfamilies. *J Leukoc Biol* **60**, 555-562 (1996).

86. Vick, S.C., Kolupaev, O.V., Perou, C.M. & Serody, J.S. Anti-PD-1 Checkpoint Therapy Can Promote the Function and Survival of Regulatory T Cells. *J Immunol* **207**, 2598-2607 (2021).

87. Kamada, T. *et al.* PD-1(+) regulatory T cells amplified by PD-1 blockade promote hyperprogression of cancer. *Proc Natl Acad Sci U S A* **116**, 9999-10008 (2019).

88. Woods, D.M. *et al.* Decreased Suppression and Increased Phosphorylated STAT3 in Regulatory T Cells are Associated with Benefit from Adjuvant PD-1 Blockade in Resected Metastatic Melanoma. *Clin Cancer Res* **24**, 6236-6247 (2018).

89. Dodagatta-Marri, E. *et al.* alpha-PD-1 therapy elevates Treg/Th balance and increases tumor cell pSmad3 that are both targeted by alpha-TGFbeta antibody to promote durable rejection and immunity in squamous cell carcinomas. *J Immunother Cancer* **7**, 62 (2019).

90. McNally, A., Hill, G.R., Sparwasser, T., Thomas, R. & Steptoe, R.J. CD4+CD25+ regulatory T cells control CD8+ T-cell effector differentiation by modulating IL-2 homeostasis. *Proc Natl Acad Sci U S A* **108**, 7529-7534 (2011).

91. Noyes, D. *et al.* Tumor-associated Tregs obstruct antitumor immunity by promoting T cell dysfunction and restricting clonal diversity in tumor-infiltrating CD8+ T cells. *J Immunother Cancer* **10** (2022).

92. Ivanova, M.E. *et al.* The pore conformation of lymphocyte perforin. *Sci Adv* **8**, eabk3147 (2022).

93. Hay, Z.L.Z. *et al.* Granzyme F: Exhaustion Marker and Modulator of Chimeric Antigen Receptor T Cell-Mediated Cytotoxicity. *J Immunol* **212**, 1381-1391 (2024).

94. Buck, M.D., Sowell, R.T., Kaech, S.M. & Pearce, E.L. Metabolic Instruction of Immunity. *Cell* **169**, 570-586 (2017).

95. O'Sullivan, D. & Pearce, E.L. Targeting T cell metabolism for therapy. *Trends Immunol* **36**, 71-80 (2015).

96. Pearce, E.L., Poffenberger, M.C., Chang, C.H. & Jones, R.G. Fueling immunity: insights into metabolism and lymphocyte function. *Science* **342**, 1242454 (2013).

97. Jellusova, J. *et al.* Gsk3 is a metabolic checkpoint regulator in B cells. *Nat Immunol* **18**, 303-312 (2017).

98. Ye, Z., Gould, T.M., Zhang, H., Jin, J., Weyand, C.M. & Goronzy, J.J. The GSK3beta-beta-catenin-TCF1 pathway improves naive T cell activation in old adults by upregulating miR-181a. *NPJ Aging Mech Dis* **7**, 4 (2021).

99. Fu, Y. *et al.* Glycogen synthase kinase 3 controls T-cell exhaustion by regulating NFAT activation. *Cell Mol Immunol* **20**, 1127-1139 (2023).

100. Joshi, N.S. *et al.* Inflammation directs memory precursor and short-lived effector CD8(+) T cell fates via the graded expression of T-bet transcription factor. *Immunity* **27**, 281-295 (2007).

101. Plumlee, C.R. *et al.* Early Effector CD8 T Cells Display Plasticity in Populating the Short-Lived Effector and Memory-Precursor Pools Following Bacterial or Viral Infection. *Sci Rep* **5**, 12264 (2015).

102. Utzschneider, D.T. *et al.* T Cell Factor 1-Expressing Memory-like CD8(+) T Cells Sustain the Immune Response to Chronic Viral Infections. *Immunity* **45**, 415-427 (2016).

103. Im, S.J. *et al.* Defining CD8+ T cells that provide the proliferative burst after PD-1 therapy. *Nature* **537**, 417-421 (2016).

104. Cramer, A. *et al.* Early-life thymectomy leads to an increase of granzyme-producing gammadelta T cells in children with congenital heart disease. *Nat Commun* **15**, 9841 (2024).

105. Ebnet, K., Levelt, C.N., Tran, T.T., Eichmann, K. & Simon, M.M. Transcription of granzyme A and B genes is differentially regulated during lymphoid ontogeny. *J Exp Med* **181**, 755-763 (1995).

106. Kummer, J.A., Kamp, A.M., Tadema, T.M., Vos, W., Meijer, C.J. & Hack, C.E. Localization and identification of granzymes A and B-expressing cells in normal human lymphoid tissue and peripheral blood. *Clin Exp Immunol* **100**, 164-172 (1995).

107. Cao, X. *et al.* Granzyme B and perforin are important for regulatory T cell-mediated suppression of tumor clearance. *Immunity* **27**, 635-646 (2007).

Acknowledgements

We thank Dale long and his team from NIH Tetramer Core Facility at Emory for providing GP33 tetramers and Fredéric Duval and Anne-Mari Aubin from the Flow Cytometry Core Facility of CR-HMR for their help.

Authors contributions

B.M. and C.E.R. designed the study. B.M., J.K, A.K., C.L.N.A.P., L.C.P., L.H, A.L.C. and H.T. performed experiments. B.M., J.K and A.K. analysed the data. B.M. and C.E.R. prepared the figures. F.S.N., R.S.S. and K.L.B.M. and C.E.R. wrote the manuscript. All

authors discussed the data and reviewed the manuscript before submission. All authors read and approved the final manuscript. C.E.R. coordinated ethical approval to work with samples at the HMR. C.E.R. and BM wrote the manuscript.

Funding

CER was supported by the Canadian Institutes of Health Research Foundation grant (159912) (PI) and National Institutes of Health grant RO1 AI049466 (co-PI). CER holds a majority stake in ImmunoAb Res Inc (Canada).

Competing interests

The authors declare no competing interests.

Additional information

Extended data is available for this paper at

Supplementary information The online version contains supplementary material available at

Correspondence and requests for materials should be addressed to

Christopher E Rudd

Peer review information Nature Cancer thanks

Reprints and permissions information is available at

Publisher's note Springer Nature remains neutral with regard to jurisdictional claims in published maps and institutional affiliations.

Open Access This article is licensed under a Creative Commons Attribution 4.0 International License, which permits use, sharing, adaptation, distribution and reproduction in any medium or format, as long as you give appropriate credit to the original author(s) and the source, provide a link to the Creative Commons licence, and indicate if changes were made. The images or other third party material in this article are included in the article's Creative Commons licence, unless indicated otherwise in a credit line to the material. If material is not included in the article's Creative Commons licence and your intended use is not permitted by statutory regulation or exceeds the permitted use, you will need to obtain permission directly from the copyright holder. To view a copy of this licence, visit http://creativecommons.org/licenses/by/4.0/.

Figure 1

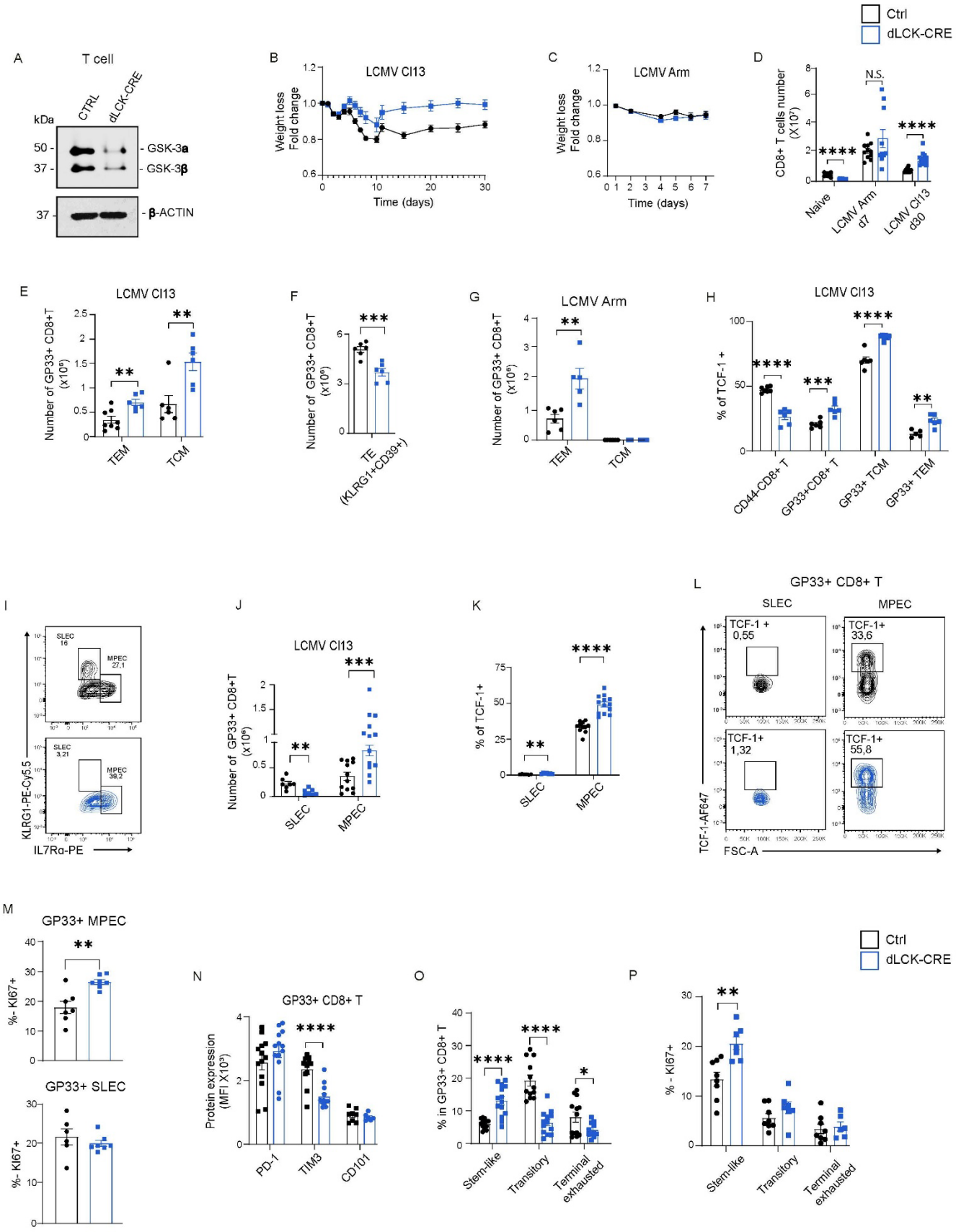
Ctrl
dLCK-CRE
A
T cell
CTRL
dLCK-CRE
kDa
50
37
GSK-3α
GSK-3β
37
β-ACTIN
B
LCMV Cl13
Weight loss Fold change
Time (days)
C
LCMV Arm
Weight loss Fold change
Time (days)
D
CD8+ T cells number (X10⁷)
N.S.
****
****
Naive
LCMV Arm d7
LCMV Cl13 d30
E
LCMV Cl13
Number of GP33+ CD8+T (x10⁶)
**
**
TEM
TCM
F
Number of GP33+ CD8+T (x10⁶)
***
TE (KLRG1+CD39+)
G
LCMV Arm
Number of GP33+ CD8+T (x10⁶)
**
TEM
TCM
H
LCMV Cl13
% of TCF-1 +
****
***
****
**
CD44-CD8+ T
GP33+CD8+ T
GP33+ TCM
GP33+ TEM
I
SLEC 16
MPEC 27,1
SLEC 3,21
MPEC 39,2
KLRG1-PE-Cy5.5
IL7Rα-PE
J
LCMV Cl13
Number of GP33+ CD8+T (x10⁶)
**
***
SLEC
MPEC
K
% of TCF-1+
**
****
SLEC
MPEC
L
GP33+ CD8+ T
SLEC
MPEC
TCF-1 + 0,55
TCF-1+ 33,6
TCF-1+ 1,32
TCF-1+ 55,8
TCF-1-AF647
FSC-A
M
GP33+ MPEC
%- Ki67+
**
GP33+ SLEC
%- Ki67+
N
GP33+ CD8+ T
Protein expression (MFI X10³)
****
PD-1
TIM3
CD101
O
% in GP33+ CD8+ T
****
****
*
Stem-like
Transitory
Terminal exhausted
P
% - Ki67+
**
Stem-like
Transitory
Terminal exhausted

Fig. 1: GSK-3 KD regulates T-cell progenitors and exhaustion. (**A**) Western blot analysis of GSK-3 expression in splenic T cells (n=3) Characterization of CD8+ T cell responses following LCMV infection. Mice were infected with LCMV clone 13 (cl13) or Armstrong strain, and spleens were harvested at day 30 or day 7 post-infection (p.i.), respectively. (**B-C**) Weight loss following infection with (**B**) LCMV-cl13 (n=14, pooled from 3 independent experiments) or (**C**) LCMV Armstrong (n=5, representative of 2 independent experiments). (**D**) Splenic CD8+ T cell counts in naive and LCMV-infected mice (Armstrong d7 p.i. and CL-13 d30 p.i.; n=6-14, pooled from ≥2 independent experiments). (**E**) Flow cytometry analysis and quantification of GP33+ CD8+ effector memory (TEM: CD62L-CD44+) and central memory (TCM: CD44+CD62L+) T cells (n=6-8, pooled from 2 independent experiments). (**F**) Quantification of GP33+ CD8+ terminal effector (KLRG1+CD39+) cells (n=6, pooled from 2 independent experiments). (**G**) Proportion of TEM and TCM among GP33+ CD8+ T cells after LCMV Armstrong infection (n=5-6, pooled from 2 independent experiments). (**H**) The precent TCF-1 expression in naive, activated GP33+, TCM, and TEM CD8+ T cells (n=5-7, representative of 2 independent experiments). (**I-J**) Flow cytometry profile (**I**) and histogram quantification (**J**) of short-lived effector cells (SLEC: KLRG1+CD127-) and memory precursor effector cells (MPEC: KLRG1-CD127+) among GP33+ CD8+ T cells (n=7-12, pooled from 2 independent experiments). (**K-L**) Percent TCF-1 expression (**K**) and representative plots (**L**) in SLEC and MPEC populations (n=7-12, pooled from 2 independent experiments). (**M**) Histogram showing Ki67 expression in SLEC and MPEC populations (n=6-7). Upper panel: GP33+MPEC+; lower panel: GP33+SLEC+ (**N**) Expression of exhaustion markers PD1, TIM3, and CD101 on GP33+ CD8+ T cells (n=12-14, pooled from 2 independent experiments). (**O**) Distribution of stem-like (TIM3-TCF1+), transitory (CX3CR1+TIM3+CD101-), and terminal exhausted (CX3CR1-TIM3+CD101+) cells among PD1+GP33+ CD8+ T cells (n=12-14, pooled from ≥2 independent experiments). (**P**) Ki67 expression in stem-like, transitory, and terminal exhausted populations (n=7-8). Data presented as mean ± SEM. Statistical significance determined by unpaired t-test: *p<0.05, **p<0.01, ***p<0.001, ****p<0.0001; NS, not significant.

Figure 2

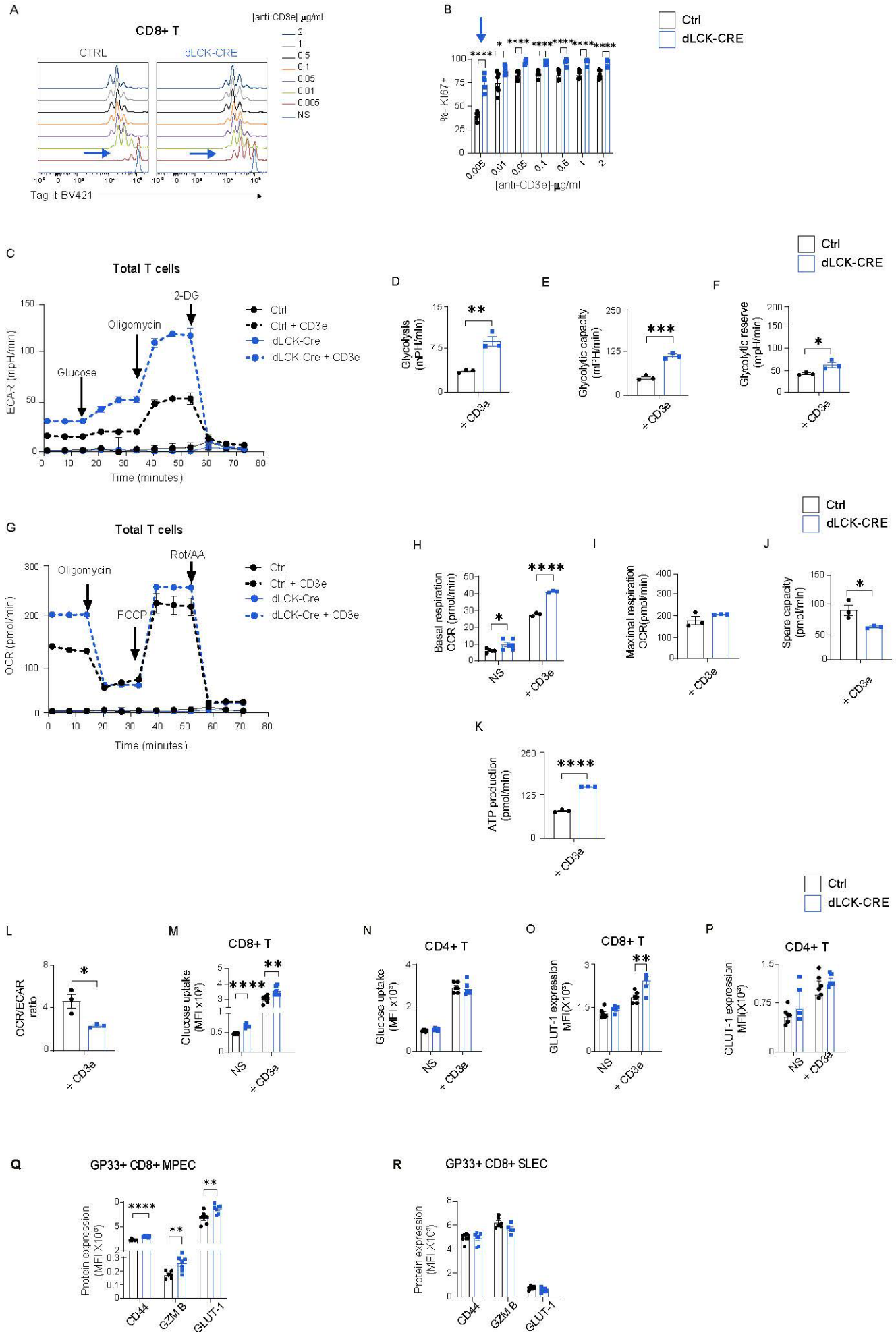
A
CD8+ T
CTRL
dLCK-CRE
[anti-CD3e]-µg/ml
2
1
0.5
0.1
0.05
0.01
0.005
NS
Tag-it-BV421
B
Ctrl
dLCK-CRE
%- Ki67+
[anti-CD3e]-µg/ml
C
Total T cells
Glucose
Oligomycin
2-DG
ECAR (mpH/min)
Time (minutes)
Ctrl
Ctrl + CD3e
dLCK-Cre
dLCK-Cre + CD3e
D
Glycolysis (mPH/min)
+ CD3e
E
Glycolytic capacity (mPH/min)
F
Glycolytic reserve (mpH/min)
G
Total T cells
Oligomycin
FCCP
Rot/AA
OCR (pmol/min)
H
Basal respiration OCR (pmol/min)
NS
I
Maximal respiration OCR(pmol/min)
J
Spare capacity (pmol/min)
K
ATP production (pmol/min)
L
OCR/ECAR ratio
M
CD8+ T
Glucose uptake (MFI x10³)
N
CD4+ T
O
GLUT-1 expression MFI(X10³)
P
Q
GP33+ CD8+ MPEC
Protein expression (MFI X10³)
CD44
GZM B
GLUT-1
R
GP33+ CD8+ SLEC

Fig. 2: Metabolic profiling of T cells from WT and dLCK-CRE mice.(**A**) Representative flow cytometry plots of Tag-it staining in splenic CD8+ T cells stimulated with varying concentrations of anti-CD3ε monoclonal antibodies (mAbs) for 48 hours. (**B**) Proportion of KI67+ cells among CD8+ T cells, with blue arrow indicating lowest anti-CD3ε mAb concentration tested (n=6, pooled from 2 independent experiments). (**C**) Extracellular acidification rate (ECAR) in splenic T cells following 24h activation with anti-CD3ε (1µg/mL). Sequential injections: glucose, oligomycin, and 2-DG. (**D-F**) Quantification of glycolytic parameters: glycolysis (**D**), glycolytic capacity (**E**), and glycolytic reserve (**F**) (n=3). (**G**) Oxygen consumption rate (OCR) in T cells activated with anti-CD3ε (1µg/mL) for 24h. Sequential injections: oligomycin, FCCP, and rotenone/antimycin A (Rot/AA). (**G-K**) Quantification of respiratory parameters: basal respiration, maximal respiration, spare capacity, and ATP production (n=3). (**L**) Ratio of maximal OCR to maximal ECAR. (**M-N**) Glucose uptake measured by NDBG mean fluorescence intensity (MFI) in CD8+ and CD4+ T-cells, unstimulated (NS) or activated with anti-CD3ε (1µg/mL) for 24h (n=5-6). (**O-P**) GLUT-1 expression analysis by flow cytometry in CD8+ and CD4+ T cells, unstimulated (NS) or activated with anti-CD3ε (1µg/mL) for 24h (n=5-6). Data represent mean ± SEM from 2-3 independent experiments. (**Q-R**) GLUT-1, CD44 and GZMB MFI expression analysis by flow cytometry in GP33+CD8+ MPEC+ (O) and GP33+CD8+ SLEC+ T cells (P) from LCMVCl13 infected mice (see Figure 2). Statistical analysis: unpaired t-test (*$p<0.05$, **$p<0.01$, ***$p<0.001$, ****$p<0.0001$; NS, not significant).

Figure 3

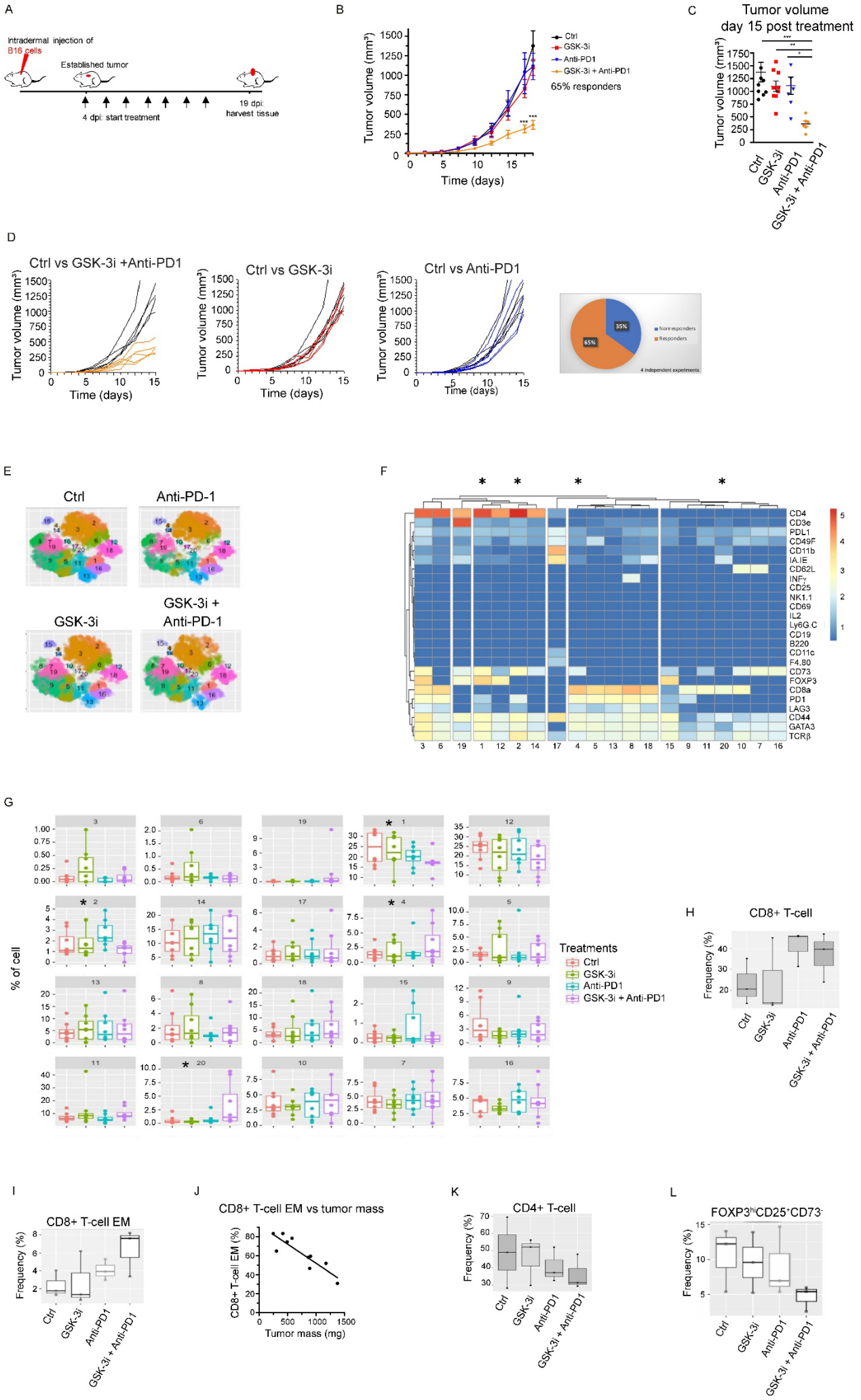
A
Intradermal injection of B16 cells
Established tumor
4 dpi: start treatment
19 dpi: harvest tissue
B
Tumor volume (mm³)
Time (days)
Ctrl
GSK-3i
Anti-PD1
GSK-3i + Anti-PD1
65% responders
C
Tumor volume day 15 post treatment
Tumor volume (mm³)
Ctrl
GSK-3i
Anti-PD1
GSK-3i + Anti-PD1
D
Ctrl vs GSK-3i +Anti-PD1
Ctrl vs GSK-3i
Ctrl vs Anti-PD1
Tumor volume (mm³)
Time (days)
35%
65%
Nonresponders
Responders
4 independent experiments
E
Ctrl
Anti-PD-1
GSK-3i
GSK-3i + Anti-PD-1
F
CD4
CD3e
PDL1
CD49F
CD11b
IA.IE
CD62L
INFγ
CD25
NK1.1
CD69
IL2
Ly6G.C
CD19
B220
CD11c
F4.80
CD73
FOXP3
CD8a
PD1
LAG3
CD44
GATA3
TCRβ
G
% of cell
Treatments
Ctrl
GSK-3i
Anti-PD1
GSK-3i + Anti-PD1
H
CD8+ T-cell
Frequency (%)
I
CD8+ T-cell EM
Frequency (%)
J
CD8+ T-cell EM vs tumor mass
CD8+ T-cell EM (%)
Tumor mass (mg)
K
CD4+ T-cell
Frequency (%)
L
FOXP3hiCD25+CD73-
Frequency (%)

Fig. 3: GSK-3 SMI enable CD8 + super-armed killers T cells in anti-PD-1 immunotherapy. (**A**) Schematic of experimental design. (**B,C**) Tumor volume quantification at day 16 post-implementation under indicated conditions (n=5-10, data pooled from ≥2 independent experiments). (**D**) Upper panel: Representative spider plots showing tumor progression; Lower panel: Circular plots depicting proportions of responders versus non-responders following B16F10 implantation and anti-PD1 treatment with (orange) or without GSK-3 SMI (blue) (data pooled from 4 independent experiments). (**E**) Phenograph visualization of tumor-infiltrating immune cell populations by CyTOF analysis (n=5-10). (**F**) Representative heatmap and (**G**) boxplots showing distribution of immune cell subsets identified by CyTOF. (**H**) Quantification of total CD8+ T cells and (**I**) CD8+ effector memory T cells (TEM, CD44+CD62L-) among tumor-infiltrating lymphocytes (TILs). (**J**) Correlation analysis between CD8+ TEM TIL frequency and tumor mass (n=3). (**K)** Quantification of total CD4+ T cells and (**I)** regulatory T cells (CD25+FOXP3+CD73+), respectively (n=3).

Figure 4

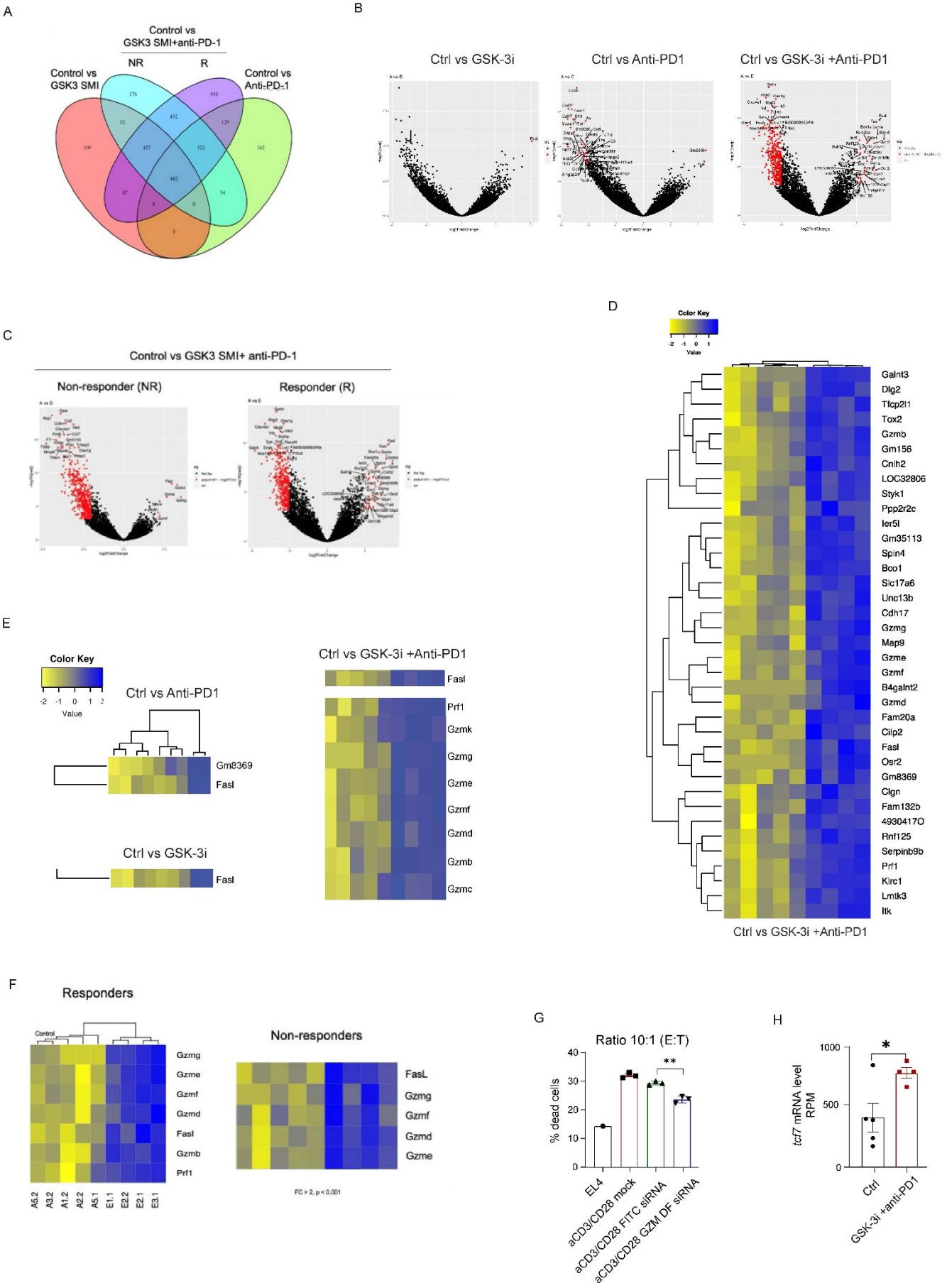
A
Control vs GSK3 SMI+anti-PD-1
NR
R
Control vs GSK3 SMI
Control vs Anti-PD-1
B
Ctrl vs GSK-3i
Ctrl vs Anti-PD1
Ctrl vs GSK-3i +Anti-PD1
C
Control vs GSK3 SMI+ anti-PD-1
Non-responder (NR)
Responder (R)
D
Color Key
Value
Galnt3
Dlg2
Tfcp2l1
Tox2
Gzmb
Gm156
Cnih2
LOC32806
Styk1
Ppp2r2c
Ier5l
Gm35113
Spin4
Bco1
Slc17a6
Unc13b
Cdh17
Gzmg
Map9
Gzme
Gzmf
B4galnt2
Gzmd
Fam20a
Cilp2
Fasl
Osr2
Gm8369
Clgn
Fam132b
4930417O
Rnf125
Serpinb9b
Prf1
Klrc1
Lmtk3
Itk
Ctrl vs GSK-3i +Anti-PD1
E
Color Key
Value
Ctrl vs Anti-PD1
Gm8369
Fasl
Ctrl vs GSK-3i
Fasl
Ctrl vs GSK-3i +Anti-PD1
Fasl
Prf1
Gzmk
Gzmg
Gzme
Gzmf
Gzmd
Gzmb
Gzmc
F
Responders
Control
Gzmg
Gzme
Gzmf
Gzmd
Fasl
Gzmb
Prf1
A5.2
A3.2
A1.2
A2.2
A5.1
E1.1
E2.2
E2.1
E3.1
Non-responders
FasL
Gzmg
Gzmf
Gzmd
Gzme
FC > 2, p < 0.001
G
Ratio 10:1 (E:T)
% dead cells
EL4
aCD3/CD28 mock
aCD3/CD28 FITC siRNA
aCD3/CD28 GZM DF siRNA
H
tcf7 mRNA level RPM
Ctrl
GSK-3i +anti-PD1

Fig. 4: GSK-3 inhibition controls CD4-CD8 cooperation in anti-PD1 cancer therapy Analysis of differentially expressed genes in CD8+ tumor-infiltrating lymphocytes (TILs). (**A**) Venn diagram of differentially expressed genes in CD8+ TILs after RNA sequencing. (**B-C**) Representative volcano plots from RNA sequencing. Genes with a log2-fold change in expression greater highlighted in red. (**D**) Representative heatmap of overexpressed genes with a log2-fold change in expression greater than 1 and a p-value of 0.001. (**E-F**) Representative heatmap of cytotoxic genes with a log2-fold change in expression greater than 1. (**G**) Quantification of the proportion of dead cells following a killing assay with GZMD and F siRNA knockdown. (**H**) Quantification of *tcf7* mRNA levels (reads per million, RPM) in CD8+ TILs. Data are shown as mean ± SEM. Statistical significance was determined by unpaired t-test (*$p < 0.05$, **$p < 0.01$, ***$p < 0.001$, ****$p < 0.0001$, NS: not significant). n = 3 with 4-5 mice per group in each experiment.

Figure 5

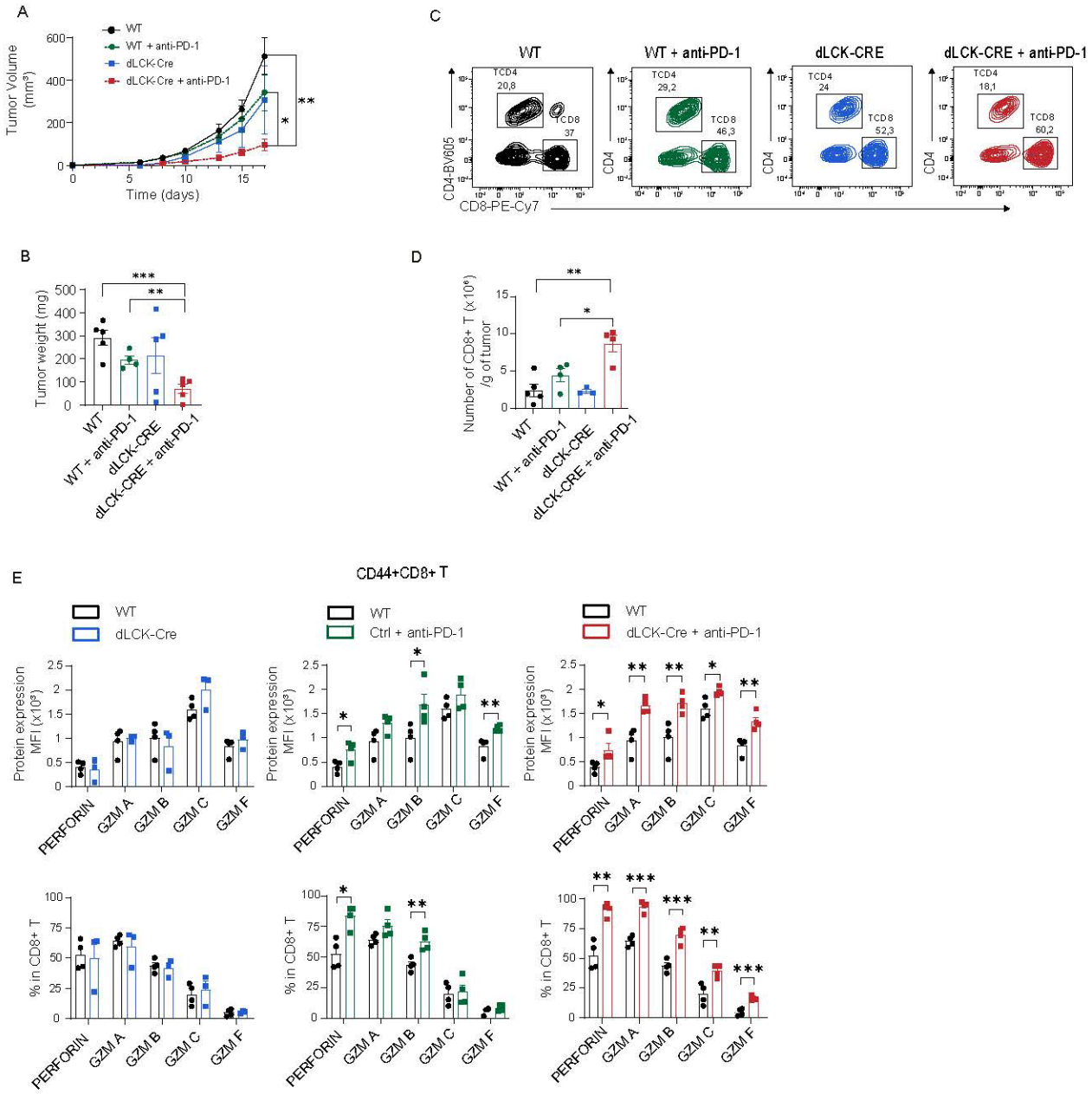

Fig. 5: GSK-3 KD also promotes anti-PD-1 synergy in generating super-armed CD8+ T-cells. B16F10 implanted WT and dLCK-CRE mice were injected or not with anti-PD1. (**A**) Tumor volume in control (ctrl) and dLck-Cre mice with or without anti-PD-1 treatment. (**B**) Tumor weight 16 days post-implantation. (**C**) Representative flow cytometry plots of CD8+ tumor-infiltrating lymphocytes (TILs). (**D**) Number of CD8+ TILs per gram of tumor tissue. **(E**) Expression and proportion of perforin, granzyme A, B, C, and F in CD44+CD8+ TILs. Data are presented as mean ± SEM. Statistical significance was determined by unpaired t-test (*p < 0.05, **p < 0.01, ***p < 0.001, ****p < 0.0001, NS: not significant). n = 3 experiments with 4--5 mice per group.

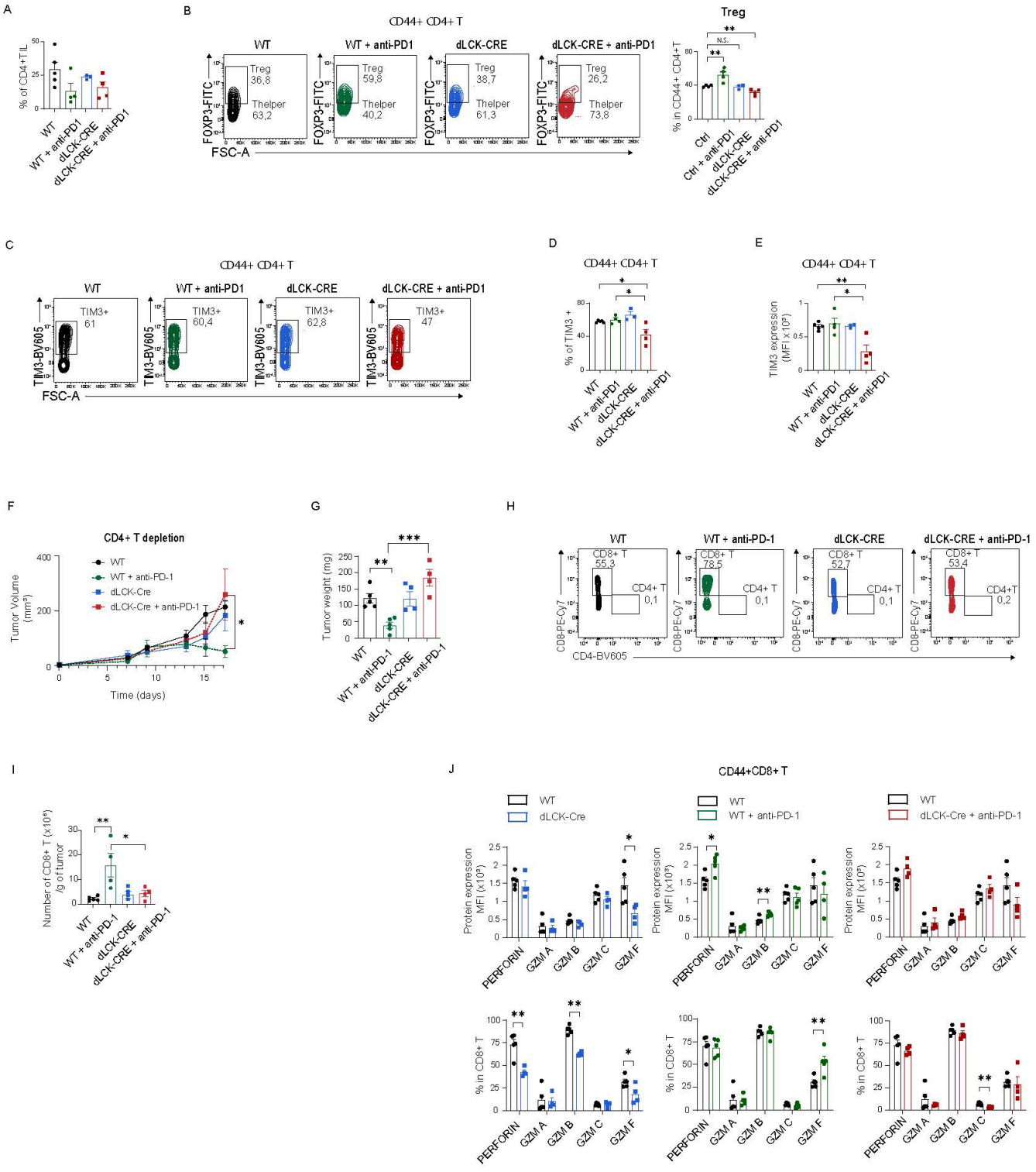
A
% of CD4+TIL
WT
WT + anti-PD1
dLCK-CRE
dLCK-CRE + anti-PD1
B
CD44+ CD4+ T
WT
WT + anti-PD1
dLCK-CRE
dLCK-CRE + anti-PD1
FOXP3-FITC
FSC-A
Treg 36,8
Thelper 63,2
Treg 59,8
Thelper 40,2
Treg 38,7
Thelper 61,3
Treg 26,2
Thelper 73,8
Treg
% in CD44+ CD4+ T
N.S.
Ctrl
Ctrl + anti-PD1
C
CD44+ CD4+ T
TIM3-BV605
TIM3+ 61
TIM3+ 60,4
TIM3+ 62,8
TIM3+ 47
D
% of TIM3 +
E
TIM3 expression (MFI x10³)
F
CD4+ T depletion
Tumor Volume (mm³)
Time (days)
WT
WT + anti-PD-1
dLCK-Cre
dLCK-Cre + anti-PD-1
G
Tumor weight (mg)
H
CD8+ T 55,3
CD4+ T 0,1
CD8+ T 78,5
CD4+ T 0,1
CD8+ T 52,7
CD4+ T 0,1
CD8+ T 53,4
CD4+T 0,2
CD8-PE-Cy7
CD4-BV605
I
Number of CD8+ T (x10⁴) /g of tumor
J
CD44+CD8+ T
dLCK-Cre
WT + anti-PD-1
dLCK-Cre + anti-PD-1
Protein expression MFI (x10³)
% in CD8+ T
PERFORIN
GZM A
GZM B
GZM C
GZM F

Fig. 6: Impact of GSK-3 on CD4+ T cells and their regulation of PD-1 blockade in anti-tumor immunity. (**A**) Quantification of CD4+ tumor-infiltrating lymphocytes (TILs) in wild-type (WT) and dLCK-Cre mice with or without anti-PD-1 treatment. (**B**) Representative flow cytometry analysis of CD4+ Treg and helper TILs in WT and dLck-Cre mice following anti-PD-1 therapy. (**C-E**) Representative flow cytometry plots (**C**) and histogram quantification **(D,E**) of TIM3+ expression on CD44+CD4+ TILs with or without anti-PD-1 treatment. (**F,G**) Tumor volume (**F**) and weight (**G**) following CD4+ T cell depletion. (**H,I**) Representative flow cytometry plots (**H**) and quantitative histogram (**I**) of CD8+ TILs after CD4+ T cell depletion. (**J**) Quantification of the loss of the induced expression of perforin, granzyme A, B, C, and F expression in CD44+CD8+ TILs after CD4+ T cell depletion in GSK-3 KD mice, shown as mean fluorescence intensity (MFI) (upper panel) and percentage (lower panel). Quantification of target cell killing with or without anti-PD-1 treatment. Data are presented as mean ± SEM. Statistical significance was determined by unpaired t-test (*$p < 0.05$, **$p < 0.01$, ***$p < 0.001$, ****$p < 0.0001$, NS: not significant). n = 4-5 mice per group.